

Spacecraft Navigation Using X-Ray Pulsars

Suneel I. Sheikh* and Darryll J. Pines†

University of Maryland, College Park, Maryland 20742

and

Paul S. Ray,‡ Kent S. Wood,§ Michael N. Lovellette,¶ and Michael T. Wolff**

U.S. Naval Research Laboratory, Washington, D.C. 20375

The feasibility of determining spacecraft time and position using x-ray pulsars is explored. Pulsars are rapidly rotating neutron stars that generate pulsed electromagnetic radiation. A detailed analysis of eight x-ray pulsars is presented to quantify expected spacecraft position accuracy based on described pulsar properties, detector parameters, and pulsar observation times. In addition, a time transformation equation is developed to provide comparisons of measured and predicted pulse time of arrival for accurate time and position determination. This model is used in a new pulsar navigation approach that provides corrections to estimated spacecraft position. This approach is evaluated using recorded flight data obtained from the unconventional stellar aspect x-ray timing experiment. Results from these data provide first demonstration of position determination using the Crab pulsar.

Introduction

THROUGHOUT history, celestial sources have been utilized for vehicle navigation. Many ships have successfully sailed the Earth's oceans using only these celestial aides. Additionally, vehicles operating in the space environment may make use of celestial sources for some portion of their navigation requirements. However, most space vehicle operations rely heavily on Earth-based navigation solutions to complete their tasks.^{1–3} For vehicles operating near Earth, the current global positioning system (GPS), and similar human-developed systems, can provide a complete navigation solution comprised of referenced time, position, velocity, attitude, and attitude rate. However, these satellite systems have limited scope for operation of vehicles relatively far from Earth, or may have their service interrupted through malfunction or unforeseen circumstances. The deep space network (DSN) assists navigation of vehicles far from Earth by determining range and range rate along the line of sight from the ground radar station to the vehicle. Although accurate radial position is determined, this accuracy is reduced for the two transverse axes of position, and DSN requires extensive ground operations and scheduling. As the cost of vehicle operations continues to increase, spacecraft navigation is evolving away from Earth-based solutions toward increasingly autonomous methods.^{4,5} Autonomous celestial-based systems, which use sources at great distance from Earth, remain attractive for complementing existing systems and for developing future navigation systems. Recently discovered celestial

sources, including neutron stars, that provide stable, predictable, and unique signatures, may provide new answers to navigating throughout the solar system and beyond.

This paper describes the utilization of pulsar sources, specifically those emitting in the x-ray band, as navigation aides for spacecraft. A new method of determining position estimates along the line of sight to a pulsar is presented. This approach compares the measured to the predicted arrival time of the pulsar signal, and differences are converted to position corrections. To perform position corrections, the authors present a time transfer equation within the solar system that accounts for relativistic effects and is accurate to within a few nanoseconds.

This paper is separated into four major sections that include a brief discussion on pulsar properties and specific characteristics for several sources; feasibility and issues of pulsars for navigation; pulse time of arrival models; and pulsar-based navigation, including position correction based on pulsar time of arrival using measured data. Several methods for future study are identified.

Background

Pulsar Description and Properties

Theories of general relativity and stellar structure project that on their collapse stars with insufficient mass to create a black hole produce several types of ultradense, compact objects.^{6,7} One such proposed object is a neutron star (NS).^{8–10} This object is the result of a massive star that has exhausted its nuclear fuel and undergone a core collapse resulting in a supernova explosion, and its stellar remnant near 1.4 solar masses collapses onto itself to form a neutron star. This star is a small, extremely dense object that is roughly 20 km in diameter and is an equilibrium configuration in which nuclear effects provide support against the strong gravity. To reach this allowed equilibrium configuration the stellar constituents must be adjusted by reactions that replace electrons and protons with neutrons, hence the name neutron stars. It is postulated that a neutron star is composed of a solid outer crust of neutron-rich nuclei a few tenths of kilometer thick surrounding a superfluid core. Conservation of angular momentum during the collapse phase tends to increase greatly the rotation rate of the star. Young, newly born neutron stars typically rotate with periods on the order of tens of milliseconds, whereas older neutron stars eventually slow down to periods on the order of a several seconds. A unique aspect of this rotation is that it can be extremely stable and predictable.

Neutron stars harbor immense magnetic fields. Under the influence of these strong fields, charged particles are accelerated along the field lines to very high energies. As these charged particles move in the pulsar's strong magnetic field, powerful beams of electromagnetic waves are radiated out from the magnetic poles of the star. If

Presented as Paper 2004-109 at the AAS/AIAA 14th Space Flight Mechanics Conference, Maui, HI, 8–12 February 2004; received 10 September 2004; revision received 25 January 2005; accepted for publication 26 January 2005. Copyright © 2005 by the authors. Published by the American Institute of Aeronautics and Astronautics, Inc., with permission. Copies of this paper may be made for personal or internal use, on condition that the copier pay the \$10.00 per-copy fee to the Copyright Clearance Center, Inc., 222 Rosewood Drive, Danvers, MA 01923; include the code 0731-5090/06 \$10.00 in correspondence with the CCC.

*Ph.D. Candidate, Department of Aerospace Engineering, Building 382; sheikh@ssl.umd.edu. Senior Member AIAA.

†Professor, Department of Aerospace Engineering, Room 3154, Martin Hall; djpterp@eng.umd.edu. Associate Fellow AIAA.

‡Astrophysicist, Space Science Division, Code 7655, 4555 Overlook Avenue, Southwest; paul.ray@nrl.navy.mil.

§Head Ultraviolet X-Ray Astrophysics and Analysis Section, Space Science Division, Code 7655, 4555 Overlook Avenue, Southwest; kent.wood@nrl.navy.mil.

¶Physicist, Space Science Division, Code 7655, 4555 Overlook Avenue, Southwest; michael.lovellette@nrl.navy.mil.

**Astrophysicist, Space Science Division, Code 7655, 4555 Overlook Avenue, Southwest; michael.wolff@nrl.navy.mil.

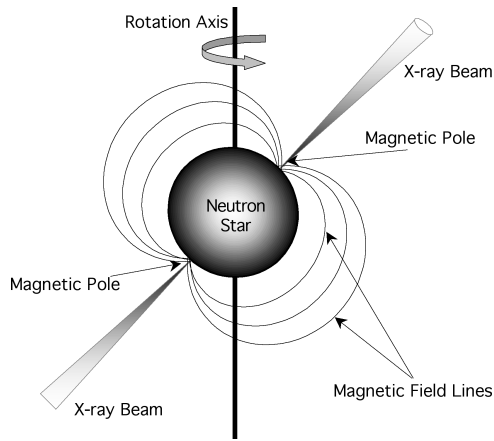


Fig. 1 Neutron star with rotation axis not aligned with its magnetic field axis.

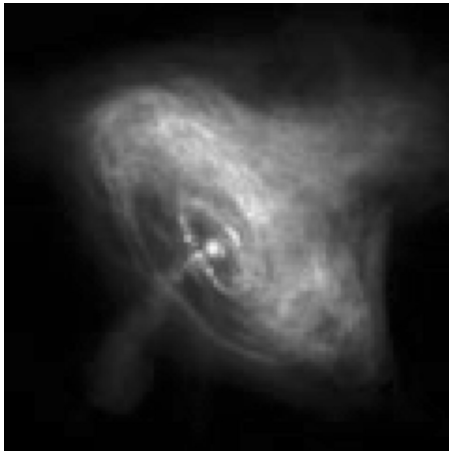


Fig. 2 Crab nebula and pulsar in x-ray band.¹²

the neutron star's spin axis is not aligned with its magnetic field axis, then an observer will sense a pulse of electromagnetic radiation as the magnetic pole sweeps across the observer's line of sight to the star. Neutron stars that exhibit this behavior are referred to as pulsars. Because no two neutron stars are formed in exactly the same manner or have the same geometric orientation relative to Earth, the pulse frequency and shape produce a unique, identifying signature for each pulsar. Thus, pulsars can act as natural beacons, or celestial lighthouses, on an intergalactic scale. Figure 1 is a diagram of a neutron star with its distinct spin and magnetic axes.

In 1967, radio pulsations were discovered during a survey of scintillation phenomena due to interplanetary plasma.¹¹ Among the expected random noise emerged a signal having a period of 1.337 s and constant to better than one part in 10^7 . Because of the extreme stability in the periodic signature, it was first conjectured that it could not be a natural signal. However, it was soon realized that these objects were neutron stars pulsating at radio frequencies. Since their discovery, pulsars have been found to emit in the radio, infrared, visible (optical), ultraviolet, x-ray, and gamma-ray energies of the electromagnetic spectrum. Figure 2 shows an image of the Crab nebula and pulsar (PSR B0531+21) taken by NASA's Chandra X-Ray Observatory. Pulsar names are typically labeled using PSR for pulsar, or an acronym for their discoverer mission, for example, X-Ray Timing Explorer (XTE), and their discovered location in right ascension (hours and minutes) and declination (degrees and minutes). Position can either be stated in the B1950 (B) or the J2000 (J) epoch coordinate frame.

Types of Pulsars

Many x-ray pulsars are rotation-powered pulsars, a neutron star whose energy source is the stored rotational kinetic energy of the star, and may exist as an isolated star or as a component of a binary

system. Two other types of pulsars, accretion-powered and anomalous, exist that are powered by different energy sources. Accretion-powered pulsars are in binary systems where material being transferred from the companion star onto the neutron star creates hot spots on the star's surface. Pulsations result from the changing viewing angle of the hot spots as the neutron star rotates. Accreting x-ray pulsars are often subdivided into those with a high-mass binary companion (HMXB, typically 10–30 solar masses) or a low-mass binary companion (LMXB, typically less than 1 solar mass). The anomalous x-ray pulsars are powered by the decay of their immense magnetic fields (approximately 10^{14} – 10^{15} Gauss) (Ref. 13).

Pulsar Stability

Because some pulsars have been observed for many years, it has been shown that the stability of their spin rates compares well to the quality of today's atomic clocks.^{14–16} Figures 3 and 4 provide comparison plots of the stability of atomic clocks and several pulsars. The metric used here for comparison is computed using third differences, $\sigma_z(t)$, or third-order polynomial variations, as opposed to second differences for the standard clock Allan variance statistic, of clock and pulsar timing residuals (see Ref. 16). This metric is sensitive to variations in frequency drift rate of atomic clocks and pulsars; the standard Allan variance is sensitive to variations in frequency drift. Older pulsars, particularly those that have undergone a long period of accretion in a binary system that spins them up to a millisecond period, have extremely stable and predictable rotation rates. Figure 4 shows data from radio pulsars; however, PSR B1937+21 is also detected in the x-ray band. Its x-ray stability is expected to be similar, or perhaps better, because of a reduction of propagation effects from the interstellar medium effect on x-ray photons.

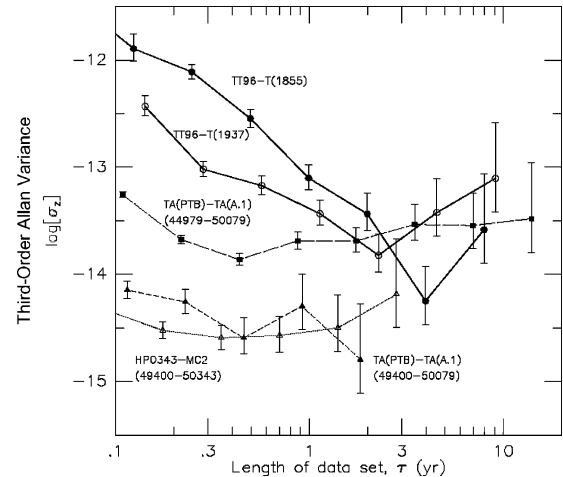


Fig. 3 Stability of atomic clocks.¹⁶

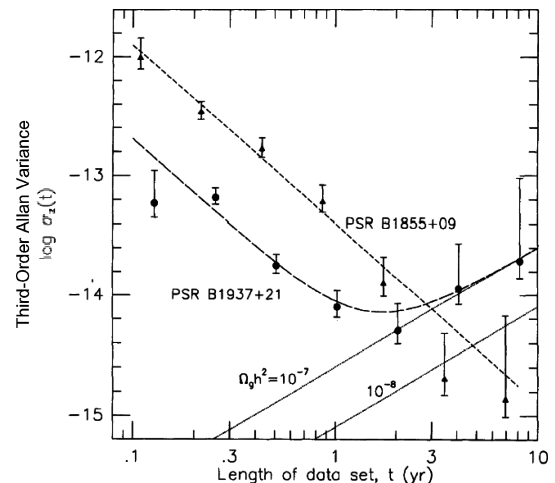


Fig. 4 Stability of pulsars.¹⁵

Additional Celestial X-Ray Sources

Pulsars exhibit many of the characteristics that make them useful as time and position navigation aides, primarily through their constant, predictable pulsations. In addition to pulsars, the x-ray sky contains other celestial objects that can be used for various aspects of spacecraft navigation.¹⁷ These objects have different energy sources that create their x-ray luminosities. Many x-ray sources are either extended or variable. However, some sources produce persistent, nonpulsating x-ray flux and are likely candidates for vehicle attitude determination.

X-Ray Catalogs

Since the discovery of the first nonsolar cosmic x-ray source of Scorpius X-1 in 1962 (Ref. 18), numerous balloon-, rocket-, and satellite-borne instruments have surveyed the x-ray sky in various energy ranges, depending on instrument characteristics or mission goals.¹⁹ The German x-ray observatory Röntgen Satellite in 2000 completed the latest comprehensive x-ray all-sky survey.^{20,21} This mission detected 18,806 bright sources (above 0.05 x-ray photon counts per second in the 0.1–2.4 keV range) and a significant number of sources, 105,924 objects, in its faint source all-sky x-ray survey.

The Australia Telescope National Facility has recently completed the most comprehensive radio pulsar study to date in their Parkes Multibeam Pulsar Survey. This survey has increased the number of known radio pulsars from 558 (Ref. 22) to over 1300 (Ref. 23). Many of these newly detected radio pulsars likely radiate in the x-ray band.

By the collection of information from literature searches and numerous x-ray survey missions, a list of candidate x-ray sources can be identified and characterized for possible use in a navigation system. The authors have assembled a catalog of such sources, and this database currently contains 759 x-ray sources, of which 69 are rotation-powered pulsars and 71 are accretion-powered pulsars. The remaining sources in this catalog are unclassified binary objects;

other variable x-ray sources, such as cataclysmic variables (CV); or extended x-ray objects, such as active galactic nebula (AGN). These additional sources with measured x-ray flux are cataloged to consider their potential use for navigation, such as attitude determination, or with further source analysis, for time, position, and/or velocity determination.

The database lists an object's characteristics, including accurate angular positions, estimated distance, x-ray fluxes and energy ranges, pulsed fraction (ratio of pulsed to nonpulsed flux from the source), pulse width [measured as full-width-half-maximum (FWHM) of main pulse], periodicities, and timing stability. The full set of x-ray sources from this catalog is plotted in galactic coordinates in Fig. 5. Distances to x-ray objects range from several to thousands of parsecs (1 parsec = 3.262 light years = 3.086×10^{16} m). Most sources are detected within the galaxy; however, as many as 45 pulsars are located outside the galaxy in the large and small Magellanic clouds (LMC and SMC, respectively), two irregular dwarf galaxies near galactic coordinates $80^\circ\text{W}-33^\circ\text{S}$ and $60^\circ\text{W}-45^\circ\text{S}$. Pulse periods range from 0.00156 to 10 s for the rotation-powered pulsars and from 0.0338 to 10,000 s for accretion-powered pulsars.

Tables 1 and 2 provide parameters of a set of pulsars from the working catalog listed with increasing pulse period. This subset of eight sources has been extracted from the catalog as a representative group of pulsar candidates that have sufficient x-ray flux, timing characteristics and stability, and geometric distribution, that potentially lend themselves to spacecraft navigation. However, this is not an exhaustive or final set of sources. Pulsar characteristics are continually updated based on new observations, which may affect a source's potential for use in navigation. A few of the recently discovered accreting sources in Tables 1 (Refs. 24–33) and 2 have not been observed sufficiently to produce period derivatives. Pulsed fraction is the value listed in the source's references, or their references. Background and nebula wind may affect the measured pulsed fraction for some sources, and so use of these values should be carefully

Table 1 List of x-ray pulsars type and position

Name	Pulsar type	Galactic longitude, °	Galactic latitude, °	Distance kiloparsec	References
PSR B1937+21	Rotation	57.51	−0.29	3.6	24, 25
PSR B1957+20	Rotation	59.20	−4.70	1.5	26, 27
XTE J1751−305	Accretion	359.18	−1.91	8	28, 29
SAX J1808.4−3658	Accretion	355.39	−8.15	4	30, 31
PSR B1821−24	Rotation	7.80	−5.58	5.5	26, 25
XTE J1807−294	Accretion	1.94	−4.27	8	32, 33
PSR B0531+21	Rotation	184.56	−5.78	2.0	26, 24
PSR B0540−69	Rotation	279.72	−31.52	47.3	26, 24

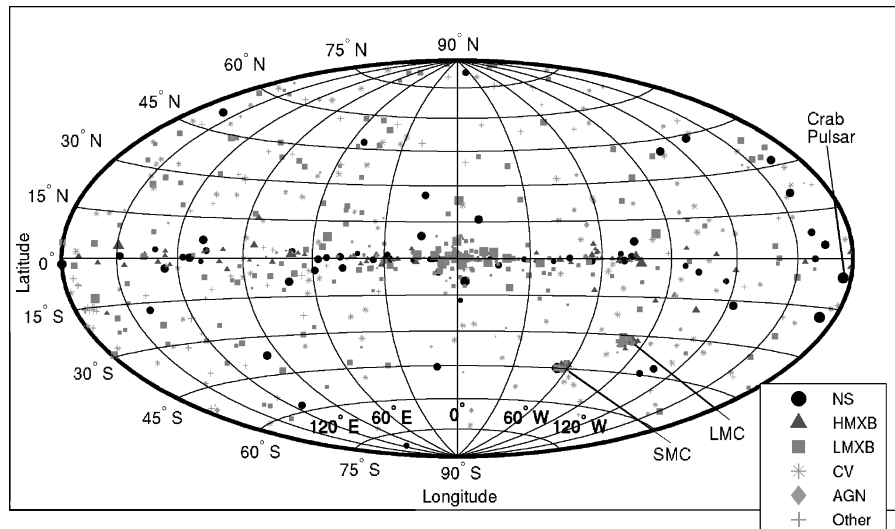


Fig. 5 X-ray sources in galactic coordinates; neutron star (NS) category includes rotation-powered and anomalous pulsars, marker size indicates relative x-ray flux intensity of each source.

Table 2 List of x-ray pulsars periodicity and pulse attributes

Name	Period, s	Period first derivative, s/s	Epoch, modified Julian date (MJD)	Flux, 2–10 keV, erg/cm ² /s	Pulsed fraction, %	Pulse width (FWHM), s
PSR B1937+21	0.00156	1.05×10^{-19}	52328.0	4.10×10^{-13}	86	2.1×10^{-5}
PSR B1957+20	0.00160	1.20×10^{-20}	48196.0	5.38×10^{-13}	60	8.0×10^{-5a}
XTE J1751–305	0.00230	1.58×10^{-18}	—	1.17×10^{-9}	5.5	5.7×10^{-4a}
SAX J1808.4–3658	0.00249	4.35×10^{-18}	—	2.13×10^{-9}	4.1	6.2×10^{-4a}
PSR B1821–24	0.00305	1.60×10^{-19}	47953.5	1.25×10^{-12}	98	5.5×10^{-5}
XTE J1807–294	0.00525	—	—	8.29×10^{-10}	7.5	1.5×10^{-3}
PSR B0531+21	0.0335	4.21×10^{-13}	48743.0	9.93×10^{-9}	70	1.7×10^{-3}
PSR B0540–69	0.0504	4.79×10^{-13}	48256.0	3.33×10^{-11}	67	2.5×10^{-3a}

^aEstimated value.

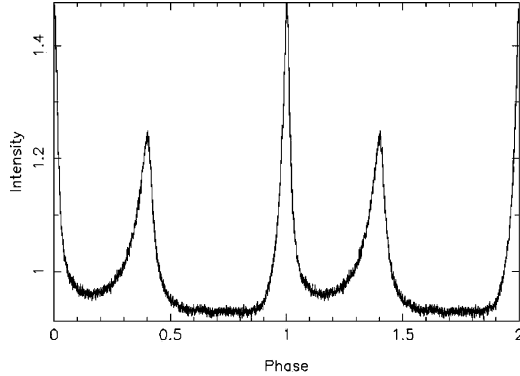


Fig. 6 Crab pulsar pulse template, period approximately 33.5 ms (epoch 51527.0 MJD); several period derivatives have been detected.

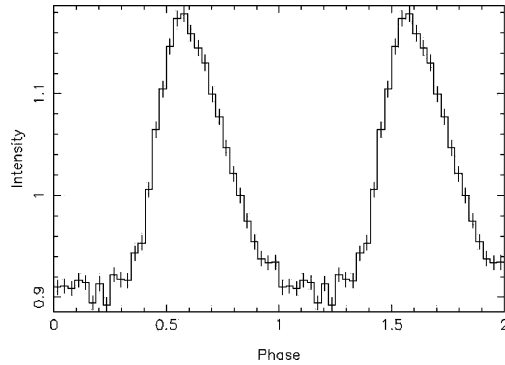


Fig. 7 PSR B1509-58 pulsar pulse template, period approximately 150.23 ms (epoch 48355.0 MJD).

considered. The estimated values of pulse width have been approximated as a fraction of pulse period, 5% for rotation-powered pulsars and 25% for accretion-powered pulsars, based on their similarity to comparable sources with measured width values.

Pulse Profiles

A pulsar pulse profile is a representation of the phase average of multiple detected pulses from a pulsar, usually shown as one or two full pulse periods. Typically, standard profile templates are created by observing a specific source over long time spans, many multiples of a pulse period, and epoch folding, or averaging synchronously with the pulse period. This folding process produces a pulse profile with a very high signal-to-noise ratio (SNR). Characteristics of the pulse can be determined from the profile, or set of profiles, including period length, amplitude, number of peaks, and variability. Figure 6 shows a standard template for the Crab pulsar (PSR B0531+21) in the x-ray band (2–10 keV). The intensity of the profile is a ratio of count rate relative to average count rate. Figure 6 shows two cycles of the pulse for clarity, and the main pulse and smaller secondary pulse are visible. Figure 7 shows a two-cycle image of the pulse profile of PSR B1509–58.

Feasibility of Pulsar-Based Navigation

Previous Research

Early researchers presented concepts for navigation using pulsars, including time determination,³⁴ and position determination for orbiting spacecraft based on radio signals from a pulsar.³⁵ However, both the radio and optical signatures from pulsars have limitations that reduce their effectiveness for spacecraft navigation. At the radio frequencies that pulsars emit (~ 100 MHz to a few gigahertz) and with their faint emissions, radio-based systems would require large antennas (on the order of 25 m in diameter or larger) to detect sources, which would be impractical for most spacecraft. Also, neighboring celestial objects including the sun, moon, Jupiter, and close stars, as well as distance objects such as radio galaxies, quasars, and the galactic diffuse emissions, are broadband radio sources that could obscure weak pulsar signals.³⁶ The small population of pulsars with detected, yet faint, optical pulsations, where only five have been identified,³⁷ severely impacts an optical pulsar-based navigation system.

During the 1970s, astronomical observations within the x-ray band of 1–20 keV (2.5×10^{17} – 4.8×10^{18} Hz) yielded pulsars with x-ray signatures. With these x-ray band signals, early postulates of x-ray sources for navigation were formed.³⁸ Although lacking supporting analysis, sensors on the order of 0.1 m² were proposed, which would be significantly smaller than the antennas or telescopes required for radio or optical observations. In the early 1990s, new proposals were presented for studying x-ray source navigation including attitude, position, and time.^{39–42} From 1999 through 2000, the U.S. Naval Research Laboratory’s (NRL) unconventional stellar aspect (USA) experiment onboard the Advanced Research and Global Observation Satellite (ARGOS) provided a platform for conducting pulsar-based spacecraft navigation experimentation.^{43,44} However, the x-ray data from this experiment were initially only used to demonstrate the concept of attitude determination.

This paper attempts to quantify expected navigation performance based on the characteristics of x-ray pulsars. This includes determining the achievable range accuracy based on source characteristics, noise effects, and observation duration. Full three-dimensional position accuracy based on observing multiple sources is also presented and demonstrated. Furthermore, detailed time transfer equations are developed that are implemented in a position correction technique to update spacecraft position, and this technique is demonstrated using actual x-ray detector data obtained from the USA experiment. Techniques for other aspects of spacecraft navigation are also discussed.

Navigation Challenges with X-Ray Sources

All celestial sources that emit sufficient detectable x-ray photons can be implemented in some manner within the spacecraft navigation scheme. Of the various x-ray sources that exist, x-ray pulsars, including rotation-powered and accretion-powered types that produce predictable pulsations, possess the most desirable characteristics for determining time and position. However, several issues complicate their use for navigation solutions. Pulsars that emit in multiple electromagnetic wavelengths do not necessarily have the same temporal signature in all observable bands. Recent studies have compared the Crab pulsar at optical, radio, and x-ray bands

and show that the pulse arrival times are dissimilar across different bands.^{45,46} Whereas a vast majority of pulsars are detectable at radio wavelengths, only a subset is seen at the optical, x-ray, and gamma-ray wavelengths. Because x rays and gamma rays are difficult to detect on the ground due to the absorption of these wavelengths by Earth's atmosphere, observations in these bands must be made above the atmosphere. The highly energetic photons emitted by the source must be detected by pointing the x-ray detector at the source, or by waiting until the source enters the field of view (FOV) of the detector. In addition, many x-ray sources are faint and require sensitive instruments to be detected. The Crab pulsar (PSR B0531+21) is the brightest rotation-powered pulsar in the x-ray band, yielding $\sim 9.9 \times 10^{-9}$ erg/cm²/s of x-ray energy flux in the 2–10 keV band. The next brightest rotation-powered pulsars are over an order of magnitude fainter than the Crab pulsar, for example, PSR B1509-58 and SAX J1846-0258 (Ref. 24). Because of the faintness of these sources, long observation times are required to produce accurate solutions. Multiple detectors may be necessary if many measurements are required within a given processing window.

Most bright x-ray sources, although located within the galaxy, are still very far from the solar system. Unlike human-made systems such as GPS, the distances to x-ray sources are not known to an accuracy that would allow absolute range determination between the source and a detector. However, the angular position in the sky can be determined with high precision, and this direction knowledge can be used in determining a navigation solution. These sources are not truly fixed in the celestial sky because they have proper motion, or radial and transverse motion relative to the solar system, although this motion is very small compared to typical source observation durations. Because many sources are clustered along the Milky Way galactic plane, a limited number of bright sources could provide off-plane triangulation for position determination.

Although pulsars are uniquely recognizable due to their different pulse shapes, a single pulse from a specific pulsar is not directly identifiable. Thus, a navigation system that updates position using the fraction of the phase cycle within a pulse must either have an a priori estimate of position to align phase approximately within a pulse, or must use additional methods to identify correctly which specific pulse is detected. The stability of pulse arrival must also be considered when creating models to predict pulse arrival times. Sources with large period derivatives must have their models updated if a long time has elapsed since the last model definition. Models that are effective for sufficiently long durations, thus requiring infrequent updates, are desirable from stable sources. Databases that contain precise models should be maintained and distributed frequently to allow users to create accurate measurements.

Though nearly all rotation-powered pulsars are constant in intensity, many accreting pulsars and most other x-ray source classes often exhibit highly aperiodic variability in intensity that may compromise their usefulness for precise time and position determination. Those in binary systems introduce more complex signal processing and pulse arrival time determination than isolated sources. Many accreting sources are unsteady, or transient, sources. This phenomenon of reduced x-ray emission for some duration is due primarily to stellar physics,⁴⁷ and the recurrence times of transient sources are often unpredictable. The accreting sources listed in Tables 1 and 2 exhibit transient characteristics, which do not allow them to be used as continuously detectable navigation source candidates. High-intensity signals lasting for short periods, x-ray flares and x-ray bursts, are occasionally detected from some sources. Because neutron stars are believed to contain a solid crust and a superfluid interior, exchanges of angular momentum between the two materials can cause unpredictable star quakes, or glitches, that can significantly alter the spin rates of these stars. The diffuse x-ray background would be present in all observations, and this would add to any noise present in the detector system.

A navigation system that uses pulsed emissions from pulsars would have to address the faintness, phase cycle, transient, flaring, bursting, and glitching aspects of these sources, in addition to the presence of the noise from the x-ray background. Although not all can be addressed in this single paper, the navigation techniques

discussed hereafter start the process of tackling these issues. This includes determining the pulse arrival time accuracy using the current knowledge of source parameters listed in Tables 1 and 2. This timing accuracy leads to range determination accuracy and is based on the computed SNR from each source.

Pulse Arrival Time Measurement

The fundamental measurable quantity of a pulsar-based navigation system is the arrival time of an observed pulse at the detector. A pulse time of arrival (TOA) measurement is generated by comparing an observed profile with a high SNR standard template profile. The observed profile $p(t)$ will differ from the template profile $s(t)$ by several factors, including a shift of time origin τ , a bias b , a scale factor k , and random noise $\eta(t)$ as in Eq. (1) (Ref. 48). Poisson counting statistics typically dominate the random noise for x-ray observations,

$$p(t) = b + k[s(t - \tau)] + \eta(t) \quad (1)$$

The observed profile is created via the detection of photons from the pulsar as they arrive at the navigation system's detector. The detector records the time of arrival of each individual x-ray photon with respect to the system clock to high precision (on the order of 1 μ s or better). During the total observation time, a large number of photons, N , will have their arrival times recorded. Individual photon arrival times from τ_0 to τ_{N-1} are then converted to their equivalent time in an inertial frame, from t_0 to t_{N-1} , as described in the following sections. This set of photons is then folded at the predicted pulse period based on the known timing model of the pulsar. A binned pulse profile is then constructed by dividing the pulse phase into M equal bins and dropping each of the N photons into the appropriate phase bin.

Converting time to phase of the pulse period, the TOA is then determined by measuring the phase offset of the observed profile with respect to the high SNR standard profile template. This is based on the assumption that, after averaging a sufficiently large number of pulses, a pulse profile recorded in the same energy range is invariant with time. The template can be aligned with an arbitrary point in the profile as phase zero, but two conventions are commonly used. Either the peak of the main pulse can be aligned as the zero phase point, or the profile can be aligned such that the phase of the fundamental component of its Fourier transform is zero. The latter method is preferred because it is more precise and generally applicable.

It is important to determine the TOA with an accuracy that is determined by the SNR of the profile and not by the choice of the bin size. A standard cross-correlation analysis does not allow this to be easily achieved. However, the method given by Taylor⁴⁸ is independent of bin size and can be implemented into a navigation system. The technique employs the time-shifting property of Fourier transform pairs. The Fourier transform of a function shifted by an amount τ is the Fourier transform of the original function multiplied by a phase factor of $e^{2\pi i f \tau}$. Because the observed profile differs from the template by a time shift, a scale factor, and random noise, as in Eq. (1), it is straightforward to transform both the profile and the template into the Fourier domain. The parameters in Eq. (1) are then easily determined by a standard least-squares fitting method. The final measured TOA of the pulse is then determined by adding the fitted offset τ to the recorded start time of the data set t_0 .

The SNR can be determined from the observed x-ray photon flux, F_X from the pulsar and B_X from the x-ray background radiation. This ratio relates the pulsed component of the signal source counts $N_{S_{\text{pulsed}}}$ to the one sigma error in detecting this signal as⁴⁹

$$\begin{aligned} \text{SNR} &= \frac{N_{S_{\text{pulsed}}}}{\sigma_{\text{noise}}} = \frac{N_{S_{\text{pulsed}}}}{\sqrt{(N_B + N_{S_{\text{nonpulsed}}}) + N_{S_{\text{pulsed}}}}} \\ &= \frac{F_X A p_f t_{\text{obs}}}{\sqrt{[B_X + F_X(1 - p_f)](A t_{\text{obs}} d) + F_X A p_f t_{\text{obs}}}} \end{aligned} \quad (2)$$

The pulsed signal component is determined by the number of photons that are received through the detector area A during the

observation time t_{obs} . The pulsed fraction p_f defines how much of the source flux is pulsed. The noise comprises the background radiation flux B_X and the nonpulsed component of the signal that is detected during the duty cycle of the pulse, plus the pulsed signal contribution. The duty cycle d of a pulse is the fraction pulse width W that spans the pulse period P , or

$$d = W/P \quad (3)$$

For a given observation, the TOA accuracy can be determined from the one sigma value of the pulse (estimated using the pulse width) and the SNR via

$$\sigma_{\text{TOA}} = \frac{1}{2}W/\text{SNR} \quad (4)$$

This accuracy represents the resolution of the arrival time of a pulse based on a single observation. A TOA measurement can be used to determine the range of the detector from a chosen reference location along the line of sight to the pulsar. The accuracy of the range measurement can be computed using c to represent the speed of light as

$$\sigma_{\text{range}} = c\sigma_{\text{TOA}} \quad (5)$$

A figure of merit (FOM) can be introduced that assists in identifying x-ray sources with the potential to provide good timing and range accuracy. When terms from the accuracy calculation in Eq. (4) that would be common to all sources for a set observation are ignored, including background, detector area, and observation time, this FOM, Q_X , can be represented as

$$Q_X = \frac{F_X p_f^2}{W^2[p_f + (W/P)(1 - p_f)]} \quad (6)$$

Using this x-ray source FOM provides a means to evaluate and rank sources that provide high-accuracy timing and range. Although this FOM is not dimensionless, it can be normalized with respect to the value of a reference candidate. By normalization with the $Q_{X_{\text{Crab}}}$ value for the Crab pulsar (PSR B0531+21), Table 3 lists the rank of the sources listed in Tables 1 and 2. Highly ranked sources have large flux and narrow pulse widths that produce accurate timing and range estimates in Eq. (5).

Figure 8 shows the achievable range measurement accuracy using the pulsar sources listed in Tables 1 and 2 and Eqs. (2–5) for SNR > 2 and a 1-m² area detector. Figure 8 shows that several sources can achieve range accuracies better than 1 km within 1000 s of observation. Figure 9 shows the range measurement accuracy plot for the same sources for a 5-m² area detector. Though it lacks the full representation of noise from Eq. (2), the listed quality ranking from Table 3 compares well with the accuracy plots shown in Figs. 8 and 9.

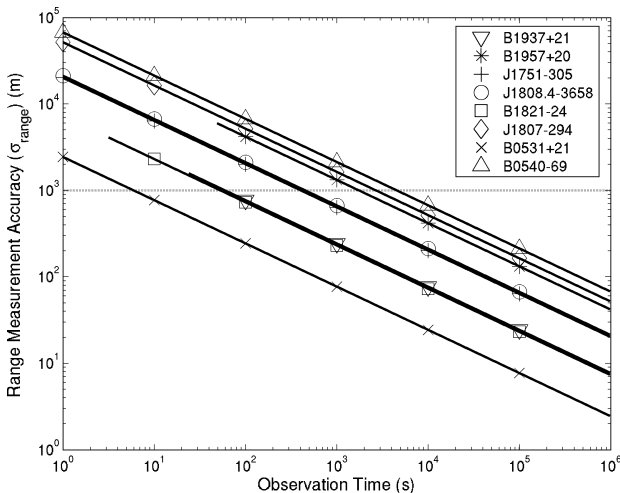


Fig. 8 Range measurement accuracies using pulsars vs observation time: area=1 m² and x-ray background= 3×10^{-11} erg/cm²/s (2–10 keV).

Table 3 FOM ranking of x-ray pulsars

Name	$Q_X/Q_{X_{\text{Crab}}}$	Rank
PSR B1937+21	0.26	2
PSR B1957+20	0.020	4
XTE J1751–305	0.015	5
SAX J1808.4–3658	0.013	6
PSR B1821–24	0.17	3
XTE J1807–294	0.0023	7
PSR B0531+21	1.00	1
PSR B0540–69	0.0014	8

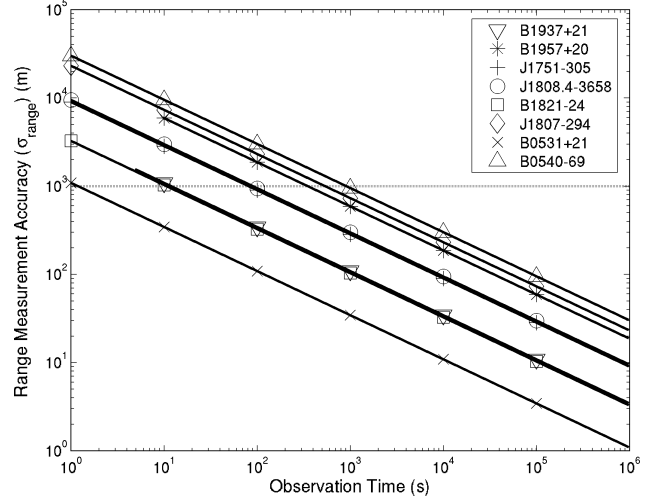


Fig. 9 Range measurement accuracies using pulsars vs observation time: area=5 m² and x-ray background= 3×10^{-11} erg/cm²/s (2–10 keV).

Figures 8 and 9 represent theoretically achievable values based on known characteristics of sources. This analysis assumes that sources have no intrinsic noise because it is not yet well understood how this noise will affect the navigation accuracy. However, a conservative estimate of x-ray background noise is used in the preceding assumptions to incorporate the effects of the pulsar signal noise and other errors that may not be fully modeled in the preceding equations. Each source is assumed to produce a single, identifiable pulse shape per pulse period, and the pulse period is assumed to be accurate over the observation duration. The analysis also assumes a perfect detector with no internal losses or noise and no background rejection. These accuracy values would change based on true characteristics of a specific detector system.

Pulsar Timing Models

The first-order analysis presented in the preceding section represents an estimate of TOA accuracies that effect position estimates. This section presents detailed TOA models and time conversion and transfer techniques. These time transfer methods include relativistic corrections to produce timing resolution of pulse photons on the order of a few nanoseconds, which in turn creates accurate TOAs.

Pulse Phase Timing Models

To compute accurate arrival times of pulses, measurements must be made relative to an inertial frame, a frame unaccelerated with respect to the pulsars.^{50–57} Because most observations are typically made on Earth, or on spacecraft moving about Earth, data collected while in a moving frame must be transferred into this inertial frame. A common inertial reference system chosen for pulsar observations is the solar system barycenter (SSB) frame with its origin at the center of mass of the solar system and uses the temps dynamique baricentrique (TDB), or barycentric dynamic time, as its time coordinate. Figure 10 shows the relationship of pulses from a pulsar as they arrive into the solar system relative to the SSB inertial frame and a spacecraft orbiting Earth. The positions of the spacecraft r

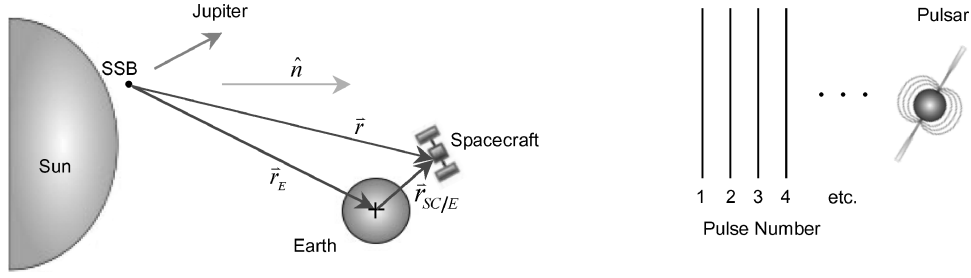


Fig. 10 Pulsar pulse arrivals within solar system.

and the center of Earth \mathbf{r}_E , with respect to the SSB, are shown, as well as the unit direction to the pulsar, $\hat{\mathbf{n}}$. Earth-based telescopes or Earth-orbiting spacecraft can reference their observations to specific epochs by initially using terrestrial time standards, such as coordinated universal time, or temps atomique international, International Atomic Time. Standard corrections can then be applied to convert recorded terrestrial time to TDB.⁵⁸

The phase of arriving pulses Φ , measured in whole cycles and fractions of the period, can be specified at the SSB using a pulsar phase model of

$$\Phi(t) = \Phi(t_0) + f[t - t_0] + (\dot{f}/2)[t - t_0]^2 + (\ddot{f}/6)[t - t_0]^3 \quad (7)$$

Equation (7) is known as the pulsar spin equation, or pulsar spindown law, with observation time t in TDB coordinate time.^{59,60} The model in Eq. (7) uses frequency f ; however, the model can also be represented using period P (also angular velocity $\Omega = 2\pi f$) as

$$\Phi(t) = \Phi(t_0) + (1/P)[t - t_0] - (\dot{P}/2P^2)[t - t_0]^2 + (\ddot{P}^2/3P^3 - \ddot{P}/6P^2)[t - t_0]^3 \quad (8)$$

The model parameters for a particular pulsar are generated through repeated observations of the source until a parameter set is created that adequately fits the observed data. The accuracy of the model prediction depends on the quality of the known timing model parameters and on the intrinsic noise of the pulsar rotation. For instance, the Jodrell Bank Observatory performs daily radio observations of the Crab pulsar and has published a monthly ephemeris report since May 1988 (Ref. 61).

The pulsar phase model of Eq. (7) or Eq. (8) allows the determination of the phase of a pulse signal at a future time t , relative to a reference epoch t_0 . The model shown in Eq. (7) utilizes pulse frequency and two of its derivatives; however, any number of derivatives may be required to model accurately a particular pulsar's timing behavior. Many more parameters may be required for some pulsars, such as those in binary systems. As long as these parameters can be sufficiently determined, any source with detectable pulsations can be used in the time and position determination schemes.

Time Corrections for Offset from Barycenter

The phase model of Eq. (7) provides a method to predict the expected arrival time of the peak amplitude of a pulsar signal at the SSB origin. To compare the measured pulse TOA at the spacecraft with the predicted pulse TOA of the model at the SSB origin, the measured TOA must be converted into the SSB inertial frame and projected to the SSB origin. This projection, or time transfer, must at least account for the time delay due to the position offset of the station from the SSB.

Proper Time to Coordinate Time Conversion

To produce an accurate navigation system, the effects on time measured by a clock in motion and within a gravitational potential field must be considered. The general relativistic theory of gravity provides a method for precisely comparing the time measured by a spacecraft's clock to a standard time reference, specifically TDB. Reference standard time, referred to as coordinate time, is the time measured by a standard clock at rest in the inertial frame.

A spacecraft's clock, which is in motion and at a different gravitational potential than the standard clock, measures proper time, or the time a clock measures as it travels along a four-dimensional space/time path. A method to convert spacecraft clock proper time to TDB coordinate time and account for high-order relativistic effects is provided hereafter.^{50–54,62–64}

The proper time measured by a moving clock τ is related to the coordinate time t via

$$dt = \left[1 + U/c^2 + \frac{1}{2}(v/c)^2 \right] d\tau \quad (9)$$

to order $\mathcal{O}(1/c^2)$ with a maximum error of 10^{-12} s (Ref. 52). The total gravitational potential U acting on the spacecraft clock is the sum of the gravitational potentials of all of the bodies in the solar system and is defined in the positive sense ($U = GM/r + \text{higher-order terms}$). Here, v is the total speed of the spacecraft's local frame through the solar system. Equation (9) can be integrated to determine absolute coordinate time relative to the proper time. Various methods have been employed to solve this integral, including a vector-based solution using positions of various planetary bodies relative to the SSB^{52,53} and a solution for an Earth-based ground telescope and its clock used for pulsar timing.^{50,51} Integrating Eq. (9) over time yields

$$\begin{aligned} \int_{t_0}^t dt &= (t - t_0) = \int_{\tau_0}^{\tau} \left[1 + \frac{U}{c^2} + \frac{1}{2} \left(\frac{v}{c} \right)^2 \right] d\tau \\ &= (\tau - \tau_0) + \int_{\tau_0}^{\tau} \left[\frac{U}{c^2} + \frac{1}{2} \left(\frac{v}{c} \right)^2 \right] d\tau \end{aligned} \quad (10)$$

Equation (10) is the general conversion equation for clocks in motion. This equation can be solved based on knowledge of the spacecraft's orbit type. The speed of an Earth-orbiting spacecraft with respect to inertial space can be related to the inertial velocity of Earth \mathbf{v}_E and the relative spacecraft velocity $\dot{\mathbf{r}}_{sc/E}$ using

$$\mathbf{v}^2 = (\mathbf{v}_E + \dot{\mathbf{r}}_{sc/E}) \cdot (\mathbf{v}_E + \dot{\mathbf{r}}_{sc/E}) \quad (11)$$

If Eq. (11) is expanded, integrated by parts, and small terms are ignored ($\dot{\mathbf{r}}_{sc/E}^2 \ll v_E^2$), Eq. (10) can be simplified to

$$(t - t_0) = (\tau - \tau_0) + \int_{\tau_0}^{\tau} \left[\frac{U}{c^2} + \frac{1}{2} \left(\frac{v_E}{c} \right)^2 \right] d\tau + \frac{1}{c^2} (\mathbf{v}_E \cdot \mathbf{r}_{sc/E}) \quad (12)$$

where $v_E = \|\mathbf{v}_E\|$. The third term on the right-hand side is often referred to as the Sagnac effect and is the correction applied to elapsed time of a light signal in a rotating reference frame, in this case, the spacecraft's clock in orbit about Earth.⁶³ For a spacecraft in orbit about another planetary body, Eq. (12) can be represented using the body's absolute velocity \mathbf{v}_{PB} and the spacecraft's relative position $\mathbf{r}_{sc/PB}$ as

$$(t - t_0) = (\tau - \tau_0) + \int_{\tau_0}^{\tau} \left[\frac{U}{c^2} + \frac{1}{2} \left(\frac{v_{PB}}{c} \right)^2 \right] d\tau + \frac{1}{c^2} (\mathbf{v}_{PB} \cdot \mathbf{r}_{sc/PB}) \quad (13)$$

For spacecraft on heliocentric orbits, the velocity term can be converted using the vis-viva energy, or energy integral, equation of the orbit.⁵² The integral can then be directly evaluated using the eccentric anomaly angle E such that

$$(t - t_0) = (\tau - \tau_0)(1 - \mu_S/2c^2a) + (2/c^2)\sqrt{a\mu_S}(E - E_0) \quad (14)$$

where $\mu_S (= GM_S)$ is the sun's gravitational parameter (and the primary gravitational influence) and a is the semimajor axis of the orbit.

Time Transfer to Solar System Barycenter

When the spacecraft's position relative to the SSB, \mathbf{r} , is used, as in Fig. 10, the offset of time a pulsar signal arrives at a spacecraft compared to the arrival time of the same pulse at the SSB to first order is

$$t_b = t_{\text{obs}} + (\hat{\mathbf{n}} \cdot \mathbf{r})/c \quad (15)$$

where t_b is the coordinate TOA at the SSB and t_{obs} is the coordinate TOA at the spacecraft. Because many pulsars are so distant from Earth, in this simple expression, the unit direction to the pulsars may be considered constant throughout the solar system. However, parallax and any apparent proper motion should be included when determining the direction of closer pulsars.

A time transfer equation with improved accuracy over Eq. (15) can be created using relativistic theory that relates the emission time of photons emanating from a source to their arrival time at a station as the photons travel through curved spacetime.^{50,51} If the performance goal of a navigation system is to provide position information on the order of less than 300 m, then the system must accurately time pulses to better than $1 \mu\text{s}$ ($\approx 300 \text{ m}/c$). The relativistic effects on time transfer neglected in Eq. (15) account for from tens to thousands of nanoseconds and, thus, must be included to ensure accurate time and position determination.

From general relativity in a weak gravitational field and nearly flat space, which is true for the solar system, a spacetime interval ds^2 that is invariant with respect to arbitrary transformations of coordinates, to order $\mathcal{O}(1/c)$, has been shown to be

$$ds^2 = -(1 - 2U/c^2)c^2 dt^2 + (1 + 2U/c^2)(dx^2 + dy^2 + dz^2) \quad (16)$$

Time transfer can be accomplished by using the path of light signals between these locations. The path taken by a light ray or particle in spacetime is called a world line, and, for electromagnetic signals, the world line is a null geodesic, or $ds^2 = 0$. Along this null geodesic, coordinate time is related to position to order $\mathcal{O}(1/c^2)$ from Eq. (16) as

$$c dt = (1 + 2U/c^2)\sqrt{dx^2 + dy^2 + dz^2} \quad (17)$$

Integrating Eq. (17) provides a method to determine when the N th pulse is received at the spacecraft, $t_{\text{obs},N}$, relative to when it was transmitted from the pulsar, T_N . The solution depends on the null geodesic path and the gravitational potential of bodies along this path. It includes the additional effects of pulsar motion from the time of transmission of the 0th pulse as

$$\mathbf{D}_N = \mathbf{D}_0 + \mathbf{V}(T_N - T_0) \approx \mathbf{D}_0 + \mathbf{V}(t_N - t_0) = \mathbf{D}_0 + \mathbf{V}\Delta t_N \quad (18)$$

In this model, \mathbf{D}_0 is the position at a fiducial transmission time T_0 and assumes a constant proper motion \mathbf{V} of the pulsar. This model assumes that the difference in transmission time for the N th pulse ($T_N - T_0$) is equal to the difference in reception time ($t_N - t_0$). Additional assumptions can be introduced such as that pulsars are very far away from the spacecraft, such that terms of order $\mathcal{O}(1/D_0^2)$ and higher can be ignored, and the direction to the pulsar can be estimated as $\hat{\mathbf{n}} \approx \mathbf{D}_0/\|\mathbf{D}_0\|$.

For pulsar timing analysis, the integrated solution between a pulsar and an observation spacecraft is^{50,51,55–57}

$$\begin{aligned} (t_{\text{obs},N} - t_{T_N}) &= \frac{1}{c} \hat{\mathbf{n}} \cdot (\mathbf{D}_N - \mathbf{p}_N) \\ &- \sum_{k=1}^{\text{PB}_{\text{SS}}} \frac{2GM_k}{c^3} \ell_{\text{v}} \left| \frac{\hat{\mathbf{n}} \cdot \mathbf{p}_{N_k} + p_{N_k}}{\hat{\mathbf{n}} \cdot \mathbf{D}_{N_k} + D_{N_k}} \right| + \frac{2\mu_S^2}{c^5 D_{N_y}^2} \\ &\times \left\{ \hat{\mathbf{n}} \cdot (\mathbf{D}_N - \mathbf{p}_N) \left[\left(\frac{\hat{\mathbf{n}} \cdot \mathbf{D}_N}{D_N} \right)^2 + 1 \right] + 2(\hat{\mathbf{n}} \cdot \mathbf{D}_N) \left(\frac{p_N}{D_N} - 1 \right) \right\} \\ &\left[+ D_{N_y} \left[\arctan \left(\frac{p_{N_x}}{D_{N_y}} \right) - \arctan \left(\frac{D_{N_x}}{D_{N_y}} \right) \right] \right] \end{aligned} \quad (19)$$

where \mathbf{p}_N represents the position of the spacecraft when it receives the N th pulse from the pulsar relative to the center of the sun (not SSB). The summation term in this equation is taken over all planetary bodies in the solar system PB_{SS} and their respective positions to the spacecraft \mathbf{p}_{N_k} . The third term, in braces, of Eq. (19) is the bending effects on the path due to the sun's gravitational field and is typically a small value (< 1 ns). This equation is often simplified for pulsar timing analysis because the transmission time from the pulsar, t_{T_N} , is unknown.^{59,60,65–67}

To determine the time transfer equation between the spacecraft and the SSB, it is necessary to solve Eq. (19) twice, once for the light ray path between the pulsar and the spacecraft and once for the path between the pulsar and the SSB. Differencing these two separate solutions produces

$$(t_{b,N} - T_N) - (t_{\text{obs},N} - T_N) = t_{b,N} - t_{\text{obs},N} \quad (20)$$

When the position of the SSB origin relative to the sun's center is given as \mathbf{b} and the position of the spacecraft relative to the SSB is given as \mathbf{r} (such that $\mathbf{p} = \mathbf{b} + \mathbf{r}$), from Eqs. (19) and (20) the time transfer between the spacecraft and the SSB is

$$\begin{aligned} t_{b,N} &= t_{\text{obs},N} + \frac{1}{c} \\ &\times \left[\hat{\mathbf{n}} \cdot \mathbf{r}_N - \frac{r_N^2}{2D_0} + \frac{(\hat{\mathbf{n}} \cdot \mathbf{r}_N)^2}{2D_0} + \frac{\mathbf{r}_N \cdot \mathbf{V}\Delta t_N}{D_0} - \frac{(\hat{\mathbf{n}} \cdot \mathbf{V}\Delta t_N)(\hat{\mathbf{n}} \cdot \mathbf{r}_N)}{D_0} \right] \\ &- \frac{(\mathbf{b}_N \cdot \mathbf{r}_N)}{D_0} + \frac{(\hat{\mathbf{n}} \cdot \mathbf{b}_N)(\hat{\mathbf{n}} \cdot \mathbf{r}_N)}{D_0} \\ &+ \sum_{k=1}^{\text{PB}_{\text{SS}}} \frac{2GM_k}{c^3} \ell_{\text{v}} \left| \frac{\hat{\mathbf{n}} \cdot \mathbf{r}_{N_k} + r_{N_k}}{\hat{\mathbf{n}} \cdot \mathbf{b}_{N_k} + b_{N_k}} + 1 \right| \end{aligned} \quad (21)$$

The difference of bending effect terms is small ($\ll 1$ ns) and has been dropped in Eq. (21). Because the values of proper motion, \mathbf{V} , are small, such that $\mathbf{D}_0 \gg \mathbf{V}\Delta t_N$, and the sun imposes the primary gravitational field within the solar system, the expression in Eq. (21) may be further simplified as

$$\begin{aligned} t_{b,N} &= t_{\text{obs},N} + \frac{\hat{\mathbf{n}} \cdot \mathbf{r}_N}{c} + \frac{1}{2cD_0} \left[(\hat{\mathbf{n}} \cdot \mathbf{r}_N)^2 - r_N^2 + 2(\hat{\mathbf{n}} \cdot \mathbf{b}_N)(\hat{\mathbf{n}} \cdot \mathbf{r}_N) \right. \\ &\left. - 2(\mathbf{b}_N \cdot \mathbf{r}_N) \right] + \frac{2\mu_S}{c^3} \ell_{\text{v}} \left| \frac{\hat{\mathbf{n}} \cdot \mathbf{r}_N + r_N}{\hat{\mathbf{n}} \cdot \mathbf{b}_N + b_N} + 1 \right| \end{aligned} \quad (22)$$

Ignoring the effects of the outer planets, as in Eq. (22), can cause errors as large as 200 ns depending on the photon's flight path.⁵⁰ When this equation is used within a navigation system, it is important to consider reference timescales, pulsar phase timing model definitions, and desired accuracy to ensure correct time transfer results.

The second term on the right-hand side of Eq. (22) is the first-order Doppler delay, and the third term is due to the effects of annual parallax. Together, these two terms are referred to as Roemer delay. The fourth term is the Shapiro delay effect.⁶⁸ The interstellar medium dispersion measure term, appearing as a correction to this equation for all radio observations, is considered zero ($\sim 10^{-3}$ ns) for high-frequency x-ray radiation. Equation (22) requires accurate solar system ephemeris information to provide the SSB location and

the sun's gravitational parameter. If the relativistic effects and terms of order $\mathcal{O}(1/D_0)$ are ignored, Eq. (22) reduces to the first-order approximation of Eq. (15).

The time transfer of Eq. (21) is necessary to compare the TOA of a pulse detected on a spacecraft anywhere in the solar system with the pulse phase timing model defined at the SSB origin. Pulse models can be described at any known location, such as the Earth center, Earth–moon barycenter, Mars center, or even other spacecraft locations. This time transfer equation can be used for other locations by replacing the position of the SSB, \mathbf{b} , with the known location where the pulse model is defined, for example, \mathbf{r}_E , if the model is defined at the Earth center.

Pulsar-Based Navigation

A pulsar-based navigation system would comprise a sensor to detect pulsar photons at the spacecraft, a clock onboard the vehicle to time the photons' arrival, and a database of known timing models for pulsars. Once a pulsar is identified and a pulse TOA is determined, this information can be utilized to update or determine attitude, velocity, time, and/or position. Methods to determine these navigation values are described hereafter, with attitude and velocity discussed briefly and position discussed in detail.

Attitude

Determining attitude of a spacecraft can be accomplished using pulsar observations through several methods. Persistent, or nonvariable, x-ray sources provide good candidates that can be identified due to their specific characteristics of flux and image. Pulsars are also potential source candidates if their pulse signal can be identified during the observation time window.

When a static, or fixed, detector on a spacecraft is assumed, the attitude of the vehicle can be determined by detecting a source in the sensor's FOV and comparing the resulting signal against a database of known x-ray source characteristics. Once the source is identified, its image on the detector plane determines angles within the sensor coordinate frame. The line of sight to the source is known in inertial frame coordinates, and the sensor to inertial frame transformation provides vehicle attitude. A detector pointed randomly in the sky will either detect a recognizable source or the x-ray background. For a static detector, it may take some time for a detectable source to enter its FOV, which will depend on vehicle rotation rate and FOV size. Because x rays are of very short wavelength, they cast sharp shadows such that diffraction is not the limiting factor for attitude determination. The achieved accuracy depends on the detector area, acceptable integration time, detector position resolution, and detector mask scale and distance. Plausible systems could achieve accuracies of arcminutes to arcseconds, depending on the particular design. Attitude rate information may also be derived by observing the image of a source as it slews across the detector's FOV.

Alternatively, a gimbaled sensor system can be used to scan various x-ray source locations in the sky to hasten the process of detecting a suitable source. However, a gimbal system requires a high-performance drive and control system to maintain fine pointing resolution while on a moving platform, which may impact vehicle design.

The USA experiment^{43,44} used a two-axis gimbal system to point its detector to desired source locations. During its mission, the USA experiment was used to detect an offset in the roll axis of the host ARGOS satellite by sweeping the detector past a known source. Because the vehicle attitude was incorrect by a small amount, the source detection did not occur at the expected attitude. By adjustment of the values of roll and yaw of the ARGOS vehicle, the USA detector was then reoriented and again pointed at the known source. This process was continued until satisfactory source detection occurred based on determined gimbal and vehicle attitude. This iterative, or feedback, method could be employed for attitude determination systems.

Velocity

Various mission applications may require knowledge of a vehicle's velocity, or speed and direction. Velocity can be determined using pulsar signal Doppler shift. Because pulsars transmit pulse

signals that are periodic in nature, as a spacecraft moves toward or away from the source, Doppler effects will be present in the measured pulsar signal. Second-order and higher Doppler effects may be significant depending on the pulsar signal and vehicle motion. Measuring the pulse frequency from a pulsar and comparing this to its expected model can determine the Doppler shift. The Doppler shift can then be converted to speed along the line of sight to the pulsar. Assembling measurements from several pulsars allows full three-dimensional velocity to be determined.

When any of the pulsar-based position determination methods described hereafter are used, a sequence of position estimates differentiated over time can also determine velocity. However, this type of measurement increases noise within the system and may have only limited use.

Time

An accurate clock is a fundamental component to the spacecraft navigation system. Onboard clocks provide a reference for a vehicle's process timer and are critical to onboard systems such as communications. Atomic clocks provide high-accuracy references and are typically accurate to 1 part in 10^9 – 10^{15} in stability over a day.¹⁶ To track the motion of radio signals at accuracies of a few tenths of a meter, a clock with nanosecond accuracy is needed.¹ This requires the clock to be stable to within 1 part in 10^{13} over several hours.

Perhaps the most significant benefit of pulsars is to provide accurate atomic clock quality time based solely on celestial observation.³⁴ The pulse arrival at the spacecraft provides a periodic signal that can be used to stabilize an onboard clock to meet the clock requirements for tracking communication signals. Detecting pulsations from celestial sources does not provide a direct measurement of absolute time; however, the stable pulsations can adjust the drift of spacecraft's clocks to maintain accurate time.

A method of correcting clock time using a phase-locked loop can be implemented.⁴⁰ In this feedback loop, the phase difference between the local clock's oscillator and the reference signal from the pulsar is driven toward zero. When repeated pulsar observations are used, the phase differences are continuously computed and any local clock errors are removed.

Alternatively, pulse TOAs can be used to correct clock time. For a spacecraft clock that is in error, the offset of the measured arrival time to the predicted arrival time provides a measure of this error. Given initial estimates of clock bias, scale factor, and jitter (b_C , k_C , and j_C), a Kalman filter can be created to update these estimates. True time τ_T can be represented using the spacecraft clock time τ_C with respect to a reference time τ_0 by

$$\tau_T = \tau_C + b_C + k_C(\tau_C - \tau_0) + \frac{1}{2}j_C(\tau_C - \tau_0)^2 + \eta_C(\tau) \quad (23)$$

The measurement provided to this filter would be the offset between the estimated clock error and the computed clock error,

$$\delta\tilde{\tau} = \tau_T - \tau_C \approx b_C + k_C(\tau_C - \tau_0) + \frac{1}{2}j_C(\tau_C - \tau_0)^2 \quad (24)$$

$$\delta\tau = \tau_p - \tau_C \quad (25)$$

True time can be estimated using τ_p , the predicted pulse arrival time from one, or several, pulsars by the use of Eq. (7).

Position

Because of the unique, periodic signatures of pulsars, it is possible to determine the position of a spacecraft. Position is determined relative to a desired inertial frame. Although the SSB provides one such frame and reference origin, it is also useful for mission operations to relate vehicle position to Earth's position as well. Several methods of position determination relative to Earth are provided hereafter. Methods for determining the position of spacecraft on interplanetary missions can be extended from the following examples. The first two methods are discussed briefly because they are similar to optical-based celestial navigation; however, they offer an advantage over optical systems because x-ray signals are difficult to blind in a conventional manner. The two methods that use accurate pulse TOA measurements require the coordinate time conversion and the barycenter offset corrections to be applied. However, this

requires spacecraft position knowledge to compute these corrections correctly. This presents a dilemma if trying to resolve spacecraft position and is discussed in the methods described hereafter.

Pulsar Elevation Method

Once an x-ray source has been detected, a vehicle with known inertial attitude can determine the direction to the object. By simultaneous observation of a reference planetary body, elevation angles between the source and reference body, as well as the apparent diameter of the body, can be used to determine the range of the detector relative to the body.⁶⁹ Persistent x-ray sources, as well as identifiable pulsars, are candidates for this method, and multiple sources are required for full position determination. Sensors that can detect objects within multiple wavelengths may be required: x ray for the source and optical for the planetary bodies, although Earth and the moon are bright in x-ray wavelengths on their sun-lit sides, which may allow an x-ray-only system. Because this method determines relative position with respect to the planetary body, absolute vehicle position can be determined by using the knowledge of absolute position of the body.

Earth-Limb Occultation

Occultation of an x-ray source by Earth's limb provides position information for Earth-orbiting spacecraft.^{39,69} As the vehicle revolves about the Earth in its orbit, x-ray sources move behind the limb and then reappear on the other side. The time spent behind Earth represents a chord length of Earth's disk. When the source position and Earth's dimensions are known, it is possible to determine the position of the vehicle relative to Earth. Knowledge of Earth's atmosphere is required because the x-ray signals would begin to be absorbed by the atmosphere as the source passes close to the limb.⁷⁰ This occultation method could be used about any planetary body with known dimensional parameters and positional ephemerides.

Absolute Position Determination

A navigation system that can operate in an absolute, or cold-start, mode does not require assistance from external sources, such as DSN or GPS, and is very advantageous after abnormal circumstances, such as a computer reset. If absolute spacecraft position is unknown, Eq. (21) cannot be directly used to transform spacecraft time to the SSB. To determine absolute position from pulsars, it is necessary to determine which specific integer phase cycle, or pulse period, is being detected at a certain time. When the phase of several pulsars is tracked and the pulsar line-of-sight directions are included, it is possible to determine the unique set of cycles that satisfies the combined information to compute absolute position relative to the SSB. Multiple simultaneous pulsar observations may be required for this process. Successive observations should be corrected for time differences and may be used if vehicle motion is relatively small between observations. This identification process is similar to the GPS integer cycle ambiguity-resolution method. Offering an advantage over GPS, pulsars can provide many different cycle lengths, some very small (a few milliseconds) to very large (many thousands of seconds), which assists the pulse cycle resolution method.

Delta-Correction Method

Pulsar signals received at a spacecraft are offset from those arriving at the SSB primarily by the distance between the SSB and the spacecraft, as in Fig. 10. If the accurate detector position is known, then the time offset of the arriving pulses between the detector and the SSB can be calculated. Conversely, if accurate time is known such that pulses are accurately measured at the detector, then the position offset of the detector and the SSB can be computed by comparing the pulse measurement with that predicted by the pulsar timing model. A pulsar's individual pulses are predicted to arrive at the SSB as per the model defined in Eq. (7), which determines when the N th pulse will arrive at the SSB relative to a chosen reference t_0 . As it moves away from the SSB, a spacecraft sensor will detect a pulse at a time relative to the predicted t_N based on Eq. (21). If, however, the spacecraft position is in error by some amount, using Eq. (21) to transform the detected pulse time from the spacecraft to the SSB will result in some offset in pulse TOA.

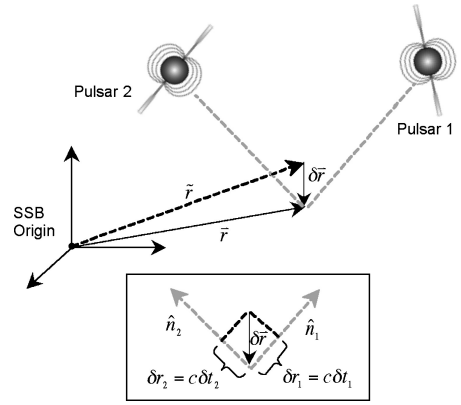


Fig. 11 Position error relative to two pulsar signals.

In the delta-correction scheme, estimated values of spacecraft position and velocity are used. Other external navigation sources, such as DSN or GPS, could generate these estimates. However, additional autonomy is provided if an onboard orbit propagator is implemented in the navigation system to provide a continuous estimate of the vehicle's dynamics during a pulsar observation. The range determined by the propagator could also be compared to the range produced from a pulsar TOA measurement. From this estimated position, \tilde{r} , the detected pulse arrival times at the spacecraft are transferred to the SSB origin via Eq. (21) and then compared to the predicted arrival times from the pulsar phase model of Eq. (7). The discrepancy in these values provides an estimate of the offset position δr . In reference to Fig. 11, the error in position will relate to a measured time offset of a pulse in the line of sight to the pulsar. Using pulsars at different locations provides line-of-sight measurements in each pulsar's direction. Combining measurements from different pulsars solves the position offset in three dimensions.

When the position offset δr is defined such that

$$\delta r = r - \tilde{r} \quad (26)$$

the errors of the predicted and measured pulse arrival times can be defined as

$$\delta t_b = t_b - \tilde{t}_b \quad (27)$$

$$\delta t_{\text{obs}} = t_{\text{obs}} - \tilde{t}_{\text{obs}} \quad (28)$$

Approximations to the nonlinear terms in Eq. (21) can be generated using Eq. (26) as

$$(\hat{n} \cdot r)^2 = (\hat{n} \cdot \tilde{r})^2 + 2(\hat{n} \cdot \tilde{r})(\hat{n} \cdot \delta r) + (\hat{n} \cdot \delta r)^2 \quad (29)$$

$$r^2 = \tilde{r} \cdot \tilde{r} + 2\tilde{r} \cdot \delta r + \delta r \cdot \delta r \quad (30)$$

$$\ln \left| \frac{\hat{n} \cdot r + r}{\hat{n} \cdot b + b} + 1 \right| = \ln \left| \frac{\hat{n} \cdot \tilde{r} + (\tilde{r} \cdot \tilde{r})^{\frac{1}{2}}}{\hat{n} \cdot b + b} + 1 \right| + \left\{ \frac{\hat{n} \cdot \delta r + (\tilde{r} \cdot \delta r) / (\tilde{r} \cdot \tilde{r})^{\frac{1}{2}}}{\left[\hat{n} \cdot \tilde{r} + (\tilde{r} \cdot \tilde{r})^{\frac{1}{2}} \right] + (\hat{n} \cdot b + b)} \right\} \quad (31)$$

With the preceding approximations in Eqs. (26–31), when terms of order $\mathcal{O}(\delta r^2)$ are considered as negligible, only the sun's gravitational field is used, and the subscript N is removed for clarity, the expression in Eq. (21) can be placed in linear form with respect to δr as

$$\delta t_b = \delta t_{\text{obs}} + \frac{\hat{n} \cdot \delta r}{c} + \frac{1}{cD_0} \left[(\hat{n} \cdot \tilde{r})(\hat{n} \cdot \delta r) - \tilde{r} \cdot \delta r + \delta r \cdot \mathbf{V} \Delta t_N - (\hat{n} \cdot \mathbf{V} \Delta t_N)(\hat{n} \cdot \delta r) - (\mathbf{b} \cdot \delta r) + (\hat{n} \cdot \mathbf{b})(\hat{n} \cdot \delta r) \right] + \frac{2\mu_S}{c^3} \left[\frac{\hat{n} \cdot \delta r + (\tilde{r} \cdot \delta r) / (\tilde{r} \cdot \tilde{r})^{\frac{1}{2}}}{\left[\hat{n} \cdot \tilde{r} + (\tilde{r} \cdot \tilde{r})^{\frac{1}{2}} \right] + (\hat{n} \cdot \mathbf{b} + b)} \right] \quad (32)$$

Equation (32) can be rewritten in vector form as

$$\delta t_b = \delta t_{\text{obs}} + \mathbf{A} \cdot \delta \mathbf{r} \quad (33)$$

The vector $\mathbf{A} = \mathbf{A}(\tilde{\mathbf{r}}, \hat{\mathbf{n}}, D_0, \mathbf{V}, \mathbf{b}, \Delta t_N)$ is composed of the terms from Eq. (32). This linear expression can be assembled for k different pulsars to create a matrix of observations,

$$\begin{bmatrix} (\delta t_b - \delta t_{\text{obs}})_1 \\ (\delta t_b - \delta t_{\text{obs}})_2 \\ \vdots \\ (\delta t_b - \delta t_{\text{obs}})_k \end{bmatrix} = \begin{bmatrix} \mathbf{A}_1^T \\ \mathbf{A}_2^T \\ \vdots \\ \mathbf{A}_k^T \end{bmatrix} \delta \mathbf{r} \quad (34)$$

The left-hand side of Eq. (34) is computed using predicted and measured arrival times of a pulse at the SSB and at the spacecraft. When the pulse model information and the propagated spacecraft position and velocity information are used, the predicted observation time \tilde{t}_{obs} of a pulse at the spacecraft can be determined relative to the current time. When the pulse is actually measured, t_{obs} , on the spacecraft, the difference of the measured and predicted time can be computed as $\delta t_{\text{obs}} = t_{\text{obs}} - \tilde{t}_{\text{obs}}$ = measured arrival time minus predicted arrival time. When the current estimate of $\tilde{\mathbf{r}}$ is used, Eq. (21) can be used to transfer the measured TOA at the spacecraft to the SSB, t_b . The predicted arrival time \tilde{t}_b of the pulse nearest to t_b can be computed using Eq. (7). The difference at the SSB can then be determined from $\delta t = t_b - \tilde{t}_b$ = measured (transferred) arrival time minus predicted (model) arrival time. When these computations and the vectors \mathbf{A} are used, Eq. (34) can be solved for $\delta \mathbf{r}$, and the estimated position of the spacecraft can be updated using Eq. (26). Repeating this measurement process refines the position estimate.

If no errors in modeling or measurement are present, then Eq. (34) solves directly for accurate position offsets. However, errors do remain that limit the performance of this system: δt_b contains errors in pulsar timing models, and time transfer δt_{obs} contains system-level timing errors and pulse signal timing errors. These errors, along with any errors in the parameters of \mathbf{A} , including pulsar position uncertainty and Earth ephemeris accuracy, contribute to the errors in $\delta \mathbf{r}$. A phase cycle ambiguity is still present because these equations can only relate to a fraction of a cycle and not to which specific cycle is being detected. Additionally, vehicle motion that is significant during the time span between the measured and predicted pulse arrival time must be addressed in an implementation of this delta-correction method. A Kalman filter incorporating vehicle dynamics and a measurement model from Eq. (33) can be used to align sequential observations to update vehicle position successfully. Additional complexity is added if one chooses to incorporate binary pulsar observations, and these extra terms must be added to Eq. (33) (Ref. 71).

Performance

To assess the potential accuracy of a pulsar-based navigation system, it is necessary to understand the error sources inherent to the system. When the observations used within the delta-correction method were derived, the time equations were linearized with respect to position error, clock error, and pulsar timing error. This linearization did not include all error sources, namely, errors in pulsar position and proper motion. When pulsar position error is added and only first-order effects from Eq. (32) are considered, the position error equation becomes

$$c(\delta t_b - \delta t_{\text{obs}}) - \delta \hat{\mathbf{n}} \cdot \tilde{\mathbf{r}} = \tilde{\mathbf{n}} \cdot \delta \mathbf{r} \quad (35)$$

Using only the first-order terms is valid in this analysis because the remaining terms are several orders of magnitude smaller.

System performance with respect to the SSB can be established using Eq. (35) based on projected estimates of error sources. The second term of the left-hand side of Eq. (35) shows that if pulsar position is not determined to high accuracy then this system's performance degrades as distance increases away from the SSB. This error growth due to distance is similar to those of Earth-based radar

Table 4 Navigation performance within solar system

Detector position, AU	Total timing error, 10^{-6} s	Pulsar position error, arcsec	Position accuracy from SSB, km
1	10	0.01	$<10^a$
1	1	0.001	$<1^a$
1	0.1	0.0001	<0.1
10	10	0.001	<10
10	1	0.0001	<1
10	0.1	0.00001	<0.1

^aCurrent day technology spans the first and second row.

range systems. Table 4 provides estimates of position performance using Eq. (35) for the pulsar-based navigation system centered at the SSB origin, which is appropriate for solar system missions. The total timing error column includes the sum of system clock errors and pulsar timing errors. Inertial frames at the barycenter of other star systems, or the galactic center, would be appropriate for interstellar missions. However, the same performance degradation would exist as vehicles travel farther from the frame's origin.

Geometric Dilution of Precision

The geometric dilution of precision (GDOP) is an expression of the accuracy of the estimated three-dimensional position.⁶³ GDOP is based on the covariance matrix of the estimated errors of the position solution produced by a given set of pulsars and provides a measure of how well the set of chosen pulsars will compute an accurate three-dimensional position. If pulsars are chosen from only one portion of the sky, the measurement matrix will skew the observations toward this direction and will not produce a good overall three-dimensional solution. If pulsars are chosen that are distributed sufficiently in the sky, then no preferred direction will skew the measurement matrix, and a good three-dimensional solution will result. Lower values of GDOP indicate more favorable pulsar distribution. For each pulsar, the relationship of spacecraft position to the measured range ρ , or phase Φ , along the line of sight to the pulsar comes from Eqs. (15) and (21) as

$$\Delta \rho_i = \lambda_i \Delta \Phi_i = c \Delta t_i = \hat{\mathbf{n}}_i \cdot \mathbf{r} \quad (36)$$

Assembling a vector of range measurements from k different pulsars produces

$$\Delta \boldsymbol{\rho} = \begin{bmatrix} \hat{\mathbf{n}}_1 \\ \hat{\mathbf{n}}_2 \\ \vdots \\ \hat{\mathbf{n}}_k \end{bmatrix} \mathbf{r} = \mathbf{H} \mathbf{r} \quad (37)$$

\mathbf{H} is referred to as the line of sight matrix. When the expectation operator E is used, and either range measurements from Eq. (37) or phase measurements are used in a similar manner, the position covariance matrix \mathbf{C} can be represented as

$$\begin{aligned} \mathbf{C} &= \text{cov}(\text{position}) = E(\mathbf{r} \cdot \mathbf{r}^T) \\ &= [(H^T H)^{-1} H^T] E(\Delta \boldsymbol{\rho} \cdot \Delta \boldsymbol{\rho}^T) [(H^T H)^{-1} H^T]^T \\ &= [(H^T H)^{-1} H^T] E(\lambda \Delta \Phi \cdot \lambda \Delta \Phi^T) [(H^T H)^{-1} H^T]^T \quad (38) \end{aligned}$$

Unlike the GPS system, which assumes the same variance for each range or phase measurement, each pulsar has unique accuracy and, thus, a different variance for its measurement, as shown in Figs. 8 and 9. However, these measurements are assumed to be uncorrelated, with zero mean, such that $E[\Delta \rho_i \cdot \Delta \rho_j] = 0$; $i \neq j$, or $E[\lambda_i \Delta \Phi_i \cdot \lambda_j \Delta \Phi_j] = 0$; $i \neq j$. Therefore, the covariance matrix for the range measurements can be expressed as the diagonal matrix

$$E[\Delta \boldsymbol{\rho} \cdot \Delta \boldsymbol{\rho}^T] = \text{diag}(\sigma_{\rho_1}^2, \sigma_{\rho_2}^2, \dots, \sigma_{\rho_k}^2) \quad (39)$$

Similarly, the covariance matrix for phase can be represented as

$$E[\lambda\Delta\Phi \cdot \lambda\Delta\Phi^T] = \text{diag}(\lambda_1^2\sigma_{\Phi_1}^2, \lambda_2^2\sigma_{\Phi_2}^2, \dots, \lambda_j^2\sigma_{\Phi_k}^2) \quad (40)$$

The position covariance matrix of Eq. (38) is a 3×3 matrix because position is a three-element vector $\mathbf{r} = \{x, y, z\}$. The GDOP can be computed from the trace of this covariance matrix, as in

$$\text{GDOP}_{\text{PSR}} = \sqrt{\text{trace}(C)} = \sqrt{\sigma_x^2 + \sigma_y^2 + \sigma_z^2} \quad (41)$$

By the use of the unit direction for position in Table 1 and the position variance from Figs. 8 and 9 after 1000 s of observation, the GDOP for all eight pulsars is 3.76 km for a 1-m² detector and 1.68 km for a 5-m² detector. If only the four pulsars B0531+21, B1821-24, B1937+21, and XTE J1751-305 are considered due to their good range variance, the GDOP improves to 1.41 km for 1 m² and 0.63 for 5 m². If the observation time is increased to 5000 s for these top four pulsars, the GDOP further improves to 0.63 km for 1 m² and 0.28 for 5 m². Because the value of $A \cdot t_{\text{obs}}$ is constant throughout the SNR expression of Eq. (2), system design tradeoffs can be considered for detector area vs observation time. For example, the SNR is the same, and, consequently, the GDOP for a 1-m² detector observing for 5000 s is the same as a 5-m² detector observing for 1000 s. However, other mitigating factors, such as power usage, may need to be considered in this type of study. The pulsars in Tables 1 and 2 all lie in the lower latitudes of the galactic sphere. Sources above the galactic equator may be considered for improved geometrical distribution, for example, XTE J0929-314 (Ref. 29).

If spacecraft clock error δt_c is observable from the pulsar range measurements, then it can also be added to the covariance state vector along with vehicle position. The equation for range measurements can be modified for this additional estimated state,

$$\Delta\rho = \begin{bmatrix} \hat{n}_1 & 1 \\ \hat{n}_2 & 1 \\ \vdots & \vdots \\ \hat{n}_j & 1 \end{bmatrix} \begin{bmatrix} \mathbf{r} \\ c\delta t_c \end{bmatrix} = H' \mathbf{r}' \quad (42)$$

where H' is the modified measurement matrix and \mathbf{r}' is new state vector that includes both spacecraft position and spacecraft clock error. The analysis for position covariance described earlier can be implemented using this new model equation of Eq. (42). The GDOP for this new system is based on the trace of the covariance matrix, but this now includes the variance due to clock error,

$$\text{GDOP}_{\text{PSR}} = \sqrt{\text{tr}(C')} = \sqrt{\sigma_x^2 + \sigma_y^2 + \sigma_z^2 + \sigma_t^2} \quad (43)$$

The position dilution of precision (PDOP) can be determined from this system by considering only the position related states as

$$\text{PDOP}_{\text{PSR}} = \sqrt{\text{tr}(C'_{3 \times 3})} = \sqrt{\sigma_x^2 + \sigma_y^2 + \sigma_z^2} \quad (44)$$

The time dilution of precision (TDOP) is directly computed by the time variance in this matrix as

$$\text{TDOP}_{\text{PSR}} = \sigma_t \quad (45)$$

Experimental Validation of Delta-Correction Method

When observations recorded by the NRL USA experiment are used, the delta-correction method described earlier can be evaluated using actual data. The USA experiment was a collimated proportional counter telescope that comprised two detectors with a FOV of 1.2×1.2 deg (FWHM). Each detector had a 1000-cm² effective area and was sensitive to photons in the 1-15 keV energy range. Only one detector was used during an observation. The USA detector was pointed to observe the Crab pulsar for multiple observations during December 1999. Table 5 lists the Crab pulsar ephemeris values used for this experiment. The observation data were recorded, including

Table 5 Crab pulsar (PSR B0531+21) ephemeris⁶¹

Parameter	Value
Right ascension (J2000)	5 h 34 min 31.972 s
Declination (J2000)	22°00'52.069''
Galactic longitude	184.5575°
Galactic latitude	-5.7843°
Distance, kiloparsec	2.0
Frequency, Hz	29.8467040932
Period, s	0.0335045369458
Frequency derivative, Hz/s	-3.7461268 × 10 ⁻¹⁰
Period derivative, s/s	4.2052296 × 10 ⁻¹³
Epoch of ephemeris, MJD	51527.0000001373958

Table 6 Position offsets from Crab pulsar observations by USA detector

Observation date	Duration, s	Observed pulse cycles	TOA difference (error), 10 ⁻⁶ s	Position offset (accuracy), km
21 Dec. 1999	446.7	13332	53.75 (5.8)	16.1 (1.8)
24 Dec. 1999	695.9	20770	-31.02 (5.2)	-9.30 (1.6)
26 Dec. 1999	421.7	12586	-37.16 (6.3)	-11.1 (1.9)

time-tagged x-ray photon detection events and ARGOS satellite 1-s navigation values. When the Crab pulsar pulse period was used, the recorded observation data were folded to produce an observed profile. Before these specific observations, several separate observations of the Crab pulsar were folded to produce a standard template profile with a high SNR. The observed profiles and the template profile were then compared as described in the preceding "Pulse Arrival Time Measurement" section to produce observation TOAs. The measured pulse TOA represents the arrival time of the peak of the first pulse within the observation window. The error in the TOA was also computed and represents the uncertainty in aligning the observed and template profiles. In the process of computing the pulse TOA, the analysis tool corrects the spacecraft recorded photon arrival time to their arrival time at the SSB as in Eq. (21). Interpolation of the navigation data was used to produce spacecraft positions at each photon arrival time. Thus, the TOA is the arrival time at the SSB origin of the measured pulse detected at the USA detector.

Spacecraft position information can now be derived from the difference between the predicted and measured pulse arrival times. If the assumption is made that any time difference is based solely on vehicle position offset in the direction of the pulsar, the error in position can be deduced from the pulsar pulse comparison. The computed position offset is the delta correction along the unit direction to the Crab pulsar based on this single TOA measurement. Table 6 lists recorded observations, their corresponding position offset determination, and estimated accuracies. Position corrections of several kilometers along the line of sight to the Crab pulsar are produced, with estimated accuracies on the order of 2 km.

A reference truth position of ARGOS was not available at the time of these 1999 observations. However, an external estimation of vehicle position was studied during January 2000. This parallel study conducted by NRL using a ground-based navigation system concluded that the ARGOS navigation calculation was in error by as much as 15 km. Further investigation is being conducted to determine why this position error existed. It has been speculated that much of this position error is due to onboard navigation system errors because during the ARGOS mission it was determined that the spacecraft's GPS receiver was faulty, and uploads every 4 h were required to correct the spacecraft's onboard orbit propagation algorithm. With these magnitudes of position error discovered for January 2000, it is likely that they existed for the observations completed during late December 1999, which could account for much of the position offset determined from the measured TOAs. Future studies are planned to simulate pulsar measurements and vehicle orbit propagation to help investigate the ARGOS navigation issues.

Table 7 Alternative applications

Application	Description
Differential/relative position	An orbiting base station could detect pulsar signals and broadcast pulse arrival times, signal errors, and updated pulsar ephemeris. ³⁵ Ideal locations for base stations include geosynchronous orbits and sun–Earth and Earth–moon Lagrange points. Spacecraft monitoring the base station’s transmissions navigate with improved accuracy with respect to the station’s location. Relative positioning from a lead vehicle could also be implemented in a satellite formation flying concept.
GPS or DSN navigation complement	X-ray pulsar navigation could complement vehicles that use the GPS and/or DSN system, or serve as a backup to human-made systems in the event of failures or catastrophes. For spacecraft above the GPS constellation, x-ray pulsar navigation could supplement obscured or unavailable GPS data. It could provide navigation information perpendicular to a radar line of sight.
GPS time complement	Pulsar-based systems could be used as time-only reference systems, such as aiding high-data rate communication.
Radio-based systems on Earth and in space	Using radio sources as celestial clocks and/or navigation aides would be a viable alternative to x-ray sources, as long as an application could support large antennas, such as on large naval vessels or a solar-sail. ³⁶
Planetary rovers	X-ray pulsar navigation could provide a navigation system for exploratory rover vehicles. A rover’s base station could monitor pulsar signals and provide relative position information for rovers that navigate over the surface terrain. Good planetary bodies candidates have a thin or negligible atmosphere, including Mars or the moon.
X-ray communication	New x-ray detector research may produce systems that can transmit and receive modulated x-ray pulses, which could carry information.

The two main computations in this experiment include the position offset calculation and its estimated accuracy. Factors that limit the position offset calculation include pulsar timing model inaccuracies, calibration errors in the USA experiment timing system, photon time binning of 32 μs in the USA data collection mode, and pulsar position errors. The reported accuracy of the Crab pulsar timing model parameters is 60 μs for the month of December 1999 (Ref. 61) and is likely a large contributor to the measured position offset. Although the USA experiment was designed to maintain a 32- μs photon bin timing accuracy, fractions of the bin size were used to improve the time resolution of arriving photons. By the use of Eq. (5), for a 0.1- m^2 detector, $\sigma_{\text{range}} = 0.3$ km for the Crab pulsar after 500 s of observation. Although this ideal computation of position accuracy is a few times less than the calculated values in Table 6, several of the aforementioned issues likely contribute to the measured accuracy. The future study of ARGOS navigation data will be made to attempt to understand this discrepancy between theoretical accuracy and recorded data accuracy to determine whether system errors or pulsar model errors dominate.

Additional Applications

The use of x-ray pulsars and other x-ray sources is not limited to single-spacecraft navigation. Other applications can be envisioned that utilize these types of sources and technology used for navigation. Table 7 lists several of these.

Conclusions

Celestial object navigation methods, which use sources at great distances from Earth, will continue to be beneficial to future space system architectures. X-ray emitting pulsars represent a small, but important, subset of all possible celestial x-ray sources. These unique sources provide pulsed radiation that can be utilized in an x-ray based navigation system for spacecraft. Given their vast distances from Earth, pulsars provide good signal coverage for operations to the moon, to Mars, throughout the solar system, and, conceivably, to the galaxy. Issues with these sources exist that makes their use complicated; however, further algorithmic and experimental study may address these complications. By the complementing of existing systems, such as GPS or DSN, this new system can increase the overall navigation performance of spacecraft missions. As shown here, the potential of these sources to determine accurate vehicle position is significant toward increased autonomy of vehicle operation. With the capability of generating a complete navigation solution, including time, position, velocity, attitude, and attitude rate, x-ray pulsars remain attractive for creating a new celestial-based spacecraft navigation system, which may be referred to as the x-ray pulsar positioning system.

Acknowledgments

Sheikh and Pines express their gratitude to the Metropolitan Washington, D.C. chapter of the Achievement Rewards for College Scientists Foundation for providing a majority of the support for this research through their fellowship program. They also express appreciation to the AIAA Foundation for its Guidance, Navigation, and Control Graduate Award in 2003 and the Aerospace Engineering Department’s Gustave J. Hokenson Fellowship for its support. Basic research in x-ray astronomy at the U.S. Naval Research Laboratory (NRL) is supported, in part, by NRL/Office of Naval Research. The authors thank those at the NRL for their assistance with this project, including Zachary Fewtrell, Jon Determan, Lev Titarchuk, and Darryl Yentis. They also thank Yong Kim of Saddleback College; Larry Vallot of the Honeywell Technology Laboratories, Stuart Bale of the University of California, Berkeley; Charles Misner of the University of Maryland; Robert Nelson of Satellite Engineering Research Corp.; David Nice of Princeton University; and Saul Rappaport and Deepto Chakrabarty of the Massachusetts Institute of Technology for their many helpful discussions and insights.

References

- Melbourne, W. G., “Navigation Between the Planets,” *Scientific American*, Vol. 234, No. 6, 1976, pp. 58–74.
- Jordan, J. F., “Navigation of Spacecraft on Deep Space Missions,” *Journal of Navigation*, Vol. 40, Jan. 1987, pp. 19–29.
- Weeks, C. J., and Bowers, M. J., “Analytical Models of Doppler Data Signatures,” *Journal of Guidance, Control, and Dynamics*, Vol. 18, No. 6, 1995, pp. 1287–1291.
- Gounley, R., White, R., and Gai, E., “Autonomous Satellite Navigation by Stellar Refraction,” *Journal of Guidance, Control, and Dynamics*, Vol. 7, No. 2, 1984, pp. 129–134.
- Folta, D. C., Gramling, C. J., Long, A. C., Leung, D. S. P., and Belur, S. V., “Autonomous Navigation Using Celestial Objects,” American Astronautical Society, Springfield, VA, 1999, pp. 2161–2177.
- Einstein, A., *The Meaning of Relativity*, Princeton Univ. Press, Princeton, NJ, 1984.
- Chandrasekhar, S., *Stellar Structure and Stellar Atmospheres*, Univ. of Chicago Press, Chicago, IL, 1989.
- Baade, W., and Zwicky, F., “Cosmic Rays from Super-novae,” *Proceedings of the National Academy of Sciences*, Vol. 20, No. 5, 1934, pp. 259–263.
- Baade, W., and Zwicky, F., “On Super-novae,” *Proceedings of the National Academy of Sciences*, Vol. 20, No. 5, 1934, pp. 254–259.
- Oppenheimer, J. R., and Volkoff, G. M., “On Massive Neutron Cores,” *Physical Review*, Vol. 55, Feb. 1939, pp. 374–381.
- Hewish, A., Bell, S. J., Pilkington, J. D. H., Scott, P. F., and Collins, R. A., “Observation of a Rapidly Pulsating Radio Source,” *Nature*, Vol. 217, Feb. 1968, pp. 709–713.
- “Time Lapse Movies of Crab Nebula,” Chandra X-Ray Observatory, NASA/Chandra X-ray Center, Smithsonian Astrophysical Observatory, URL: <http://chandra.harvard.edu/photo/2002/0052/movies.html> [cited 1 June 2003].

- ¹³Thompson, C., and Duncan, R. C., "The Soft Gamma Repeaters As Very Strongly Magnetized Neutron Stars. Part II. Quiescent Neutrino, X-ray, and Alfvén Wave Emission," *Astrophysical Journal*, Vol. 473, Dec. 1996, pp. 322–342.
- ¹⁴Rawley, L. A., Taylor, J. H., Davis, M. M., and Allan, D. W., "Millisecond Pulsar 1937+21: A Highly Stable Clock," *Science*, Vol. 238, No. 4828, 6 Nov. 1987, pp. 761–765.
- ¹⁵Kaspi, V. M., Taylor, J. H., and Ryba, M. F., "High-Precision Timing of Millisecond Pulsars. III. Long-Term Monitoring of PSRs B1855+09 and B1937+21," *Astrophysical Journal*, Vol. 428, June 1994, pp. 713–728.
- ¹⁶Matsakis, D. N., Taylor, J. H., and Eubanks, T. M., "A Statistic for Describing Pulsar and Clock Stabilities," *Astronomy and Astrophysics*, Vol. 326, Oct. 1997, pp. 924–928.
- ¹⁷Charles, P. A., and Seward, F. D., *Exploring the X-ray Universe*, Cambridge Univ. Press, 1995.
- ¹⁸Giacconi, R., Gursky, H., Paolini, F. R., and Rossi, B. B., "Evidence For X Rays From Sources Outside the Solar System," *Physical Review Letters*, Vol. 9, No. 11, 1962, pp. 439–443.
- ¹⁹"HEASARC Observatories," Laboratory for High Energy Astrophysics, NASA Goddard Space Flight Center, Greenbelt, MD, URL: <http://heasarc.gsfc.nasa.gov/docs/observatories.html> [cited 1 July 2003].
- ²⁰Voges, W., Aschenbach, B., Boller, Th., Bräuninger, H., Briel, U., Burket, W., Dennerl, K., Englhauser, J., Gruber, R., Haberl, F., Hartner, G., Hasinger, G., Kürster, M., Pfeffermann, E., Pietsch, W., Predehl, P., Rosso, C., Schmitt, J. H. M. M., Trümper, J., and Zimmerman, H. U., "The ROSAT All-Sky Survey Bright Source Catalogue (IRXS)," *Astronomy and Astrophysics*, Vol. 349, Sept. 1999, pp. 389–405.
- ²¹Voges, W., Aschenbach, B., Boller, Th., Bräuninger, H., Briel, U., Burket, W., Dennerl, K., Englhauser, J., Gruber, R., Haberl, F., Hartner, G., Hasinger, G., Pfeffermann, E., Pietsch, W., Predehl, P., Rosso, C., Schmitt, J., Trümper, J., and Zimmerman, H. U., "The ROSAT All-Sky Survey Faint Source Catalogue," International Astronomical Union Circular 7432, Central Bureau for Astronomical Telegrams, Cambridge, MA, May 2000.
- ²²Taylor, J. H., Manchester, R. N., and Lyne, A. G., "Catalog of 558 Pulsars," *Astrophysical Journal Supplemental Series*, Vol. 88, Oct. 1993, pp. 529–568.
- ²³Manchester, R. N., Lyne, A. G., Camilo, F., Bell, J. F., Kaspi, V. M., D'Amico, N., McKay, N. P. F., Crawford, F., Stairs, I. H., Possenti, A., Kramer, M., and Sheppard, D. C., "The Parkes Multi-beam Pulsar Survey—I. Observing and Data Analysis Systems, Discovery and Timing of 100 Pulsars," *Monthly Notices of the Royal Astronomical Society*, Vol. 328, Nov. 2001, pp. 17–35.
- ²⁴Possenti, A., Cerutti, R., Colpi, M., Mereghetti, S., "Re-examining The X-Ray Versus Spin-Down Luminosity Correlation of Rotation Powered Pulsars," *Astronomy and Astrophysics*, Vol. 387, June 2002, pp. 993–1002.
- ²⁵Nicastro, L., Cusumano, G., Löhmer, O., Kramer, M., Kuiper, L., Hermsen, W., Mineo, T., and Becker, W., "BeppoSAX Observation of PSR B1937+21," *Astronomy and Astrophysics*, Vol. 413, Jan. 2004, pp. 1065–1072.
- ²⁶Becker, W., and Trümper, J., "The X-Ray Luminosity of Rotation-Powered Neutron Stars," *Astronomy and Astrophysics*, Vol. 326, Oct. 1997, pp. 682–691.
- ²⁷Becker, W., and Trümper, J., "The X-Ray Emission Properties of Millisecond Pulsars," *Astronomy and Astrophysics*, Vol. 341, Jan. 1999, pp. 803–817.
- ²⁸Markwardt, C. B., Swank, J. H., Strohmayer, T. E., in 't Zand, J. J. M., and Marshall, F. E., "Discovery of a Second Millisecond Accreting Pulsar: XTE J1751-305," *Astrophysical Journal*, Vol. 575, Aug. 2002, pp. L21–L24.
- ²⁹Galloway, D. K., Chakrabarty, D., Morgan, E. H., and Remillard, R. A., "Discovery of a High-Latitude Accreting Millisecond Pulsar in a Ultracompact Binary," *Astrophysical Journal*, Vol. 576, Sept. 2002, pp. L137–L140.
- ³⁰Wijnands, R., and van der Klis, M., "A Millisecond Pulsar in an X-Ray Binary System," *Nature*, Vol. 394, July 1998, pp. 344–346.
- ³¹Chakrabarty, D., and Morgan, E. H., "The Two-Hour Orbit of a Binary Millisecond X-ray Pulsar," *Nature*, Vol. 394, July 1998, pp. 346–348.
- ³²Kirsch, M. G. F., Mukerjee, K., Breittellner, M. G., Djavidnia, S., Freyberg, M. J., Kendziorra, E., and Smith, M. J. S., "Studies of Orbital Parameters and Pulse Profile of the Accreting Millisecond Pulsar XTE J1807-294," *Astronomy and Astrophysics*, Vol. 423, Aug. 2004, pp. L9–L12.
- ³³Campana, S., Ravasio, M., Israel, G. L., Mangano, V., and Belloni, T., "XMM-Newton Observation of the 5.25 Millisecond Transient Pulsar XTE J1807-294 in Outburst," *Astrophysical Journal*, Vol. 594, Sept. 2003, pp. L39–L42.
- ³⁴Reichley, P., Downs, G., and Morris, G., "Use of Pulsar Signals As Clocks," *NASA Jet Propulsion Laboratory Quarterly Technical Review*, Vol. 1, No. 2, 1971, pp. 80–86.
- ³⁵Downs, G. S., "Interplanetary Navigation Using Pulsating Radio Sources," NASA TR N74-34150, Oct. 1974, pp. 1–12.
- ³⁶Wallace, K., "Radio Stars, What They are and The Prospects for Their Use in Navigational Systems," *Journal of Navigation*, Vol. 41, No. 3, 1988, pp. 358–374.
- ³⁷Shearer, A., Golden, A., and Beskin, G., "Implications of the Optical Observations of Isolated Neutron Stars," *Pulsar Astronomy—2000 and Beyond*, edited by M. Kramer, N. Wex, and R. Wielebinski, Astronomical Society of Pacific Conf. Series, Vol. 202, Astronomical Society of the Pacific, San Francisco, CA, 1999, pp. 307–310.
- ³⁸Chester, T. J., and Butman, S. A., "Navigation Using X-Ray Pulsars," NASA TR N81-27129, June 1981, pp. 22–25.
- ³⁹Wood, K. S., "Navigation Studies Utilizing the NRL-801 Experiment and the ARGOS Satellite," *Small Satellite Technology and Applications III*, edited by B. J. Horais, Society of Photo-Optical Instrumentation Engineers Proceedings, Vol. 1940, Bellingham, WA, 1993, pp. 105–116.
- ⁴⁰Hanson, J. E., "Principles of X-Ray Navigation," Ph.D. Dissertation, Dept. of Aeronautics and Astronautics, Stanford Univ., Stanford, CA, March 1996.
- ⁴¹Wood, K. S., Fritz, G., Hertz, P., Johnson, W. N., Kowalski, M. P., Lovellette, M. N., Wolff, M. T., Yentis, D. J., Bloom, E., Cominsky, L., Fairfield, K., Godfrey, G., Hanson, J., Lee, A., Michelson, P., Taylor, R., and Wen, H., "The USA Experiment on the ARGOS Satellite: A Low Cost Instrument for Timing X-Ray Binaries," *EUUV, X-Ray, and Gamma-Ray Instrumentation for Astronomy V*, edited by O. H. Siegmund and J. V. Vallerga, Society of Photo-Optical Instrumentation Engineers Proceedings, Vol. 2280, Bellingham, WA, 1994, p. 19.
- ⁴²Wood, K. S., Fritz, G., Hertz, P., Johnson, W. N., Lovellette, M. N., Wolff, M. T., Bloom, E., Godfrey, G., Hanson, J., Michelson, P., Taylor, R., and Wen, H., "The USA Experiment on the ARGOS Satellite: A Low Cost Instrument for Timing X-Ray Binaries," *The Evolution of X-Ray Binaries*, edited by S. S. Holt and C. S. Day, American Inst. of Physics Proceedings, Vol. 308, Melville, NY, Jan. 1994, pp. 561–564.
- ⁴³Ray, P. S., Wood, K. S., Fritz, G., Hertz, P., Kowalski, M., Johnson, W. N., Lovellette, M. N., Wolff, M. T., Yentis, D., Bandyopadhyay, R. M., Bloom, E. D., Giebels, B., Godfrey, G., Reilly, K., Saz Parkinson, P., Shabad, G., Michelson, P., Roberts, M., Leahy, D. A., Cominsky, L., Scargle, J., Beall, J., Chakrabarty, D., and Kim, Y., "The USA X-Ray Timing Experiment," *American Institute of Physics Conference Proceedings*, Vol. 599, Dec. 2001, p. 336.
- ⁴⁴Wood, K. S., Kowalski, M., Lovellette, M. N., Ray, P. S., Wolff, M. T., Yentis, D. J., Bandyopadhyay, R. M., Fewtrell, G., and Hertz, P. L., "The Unconventional Stellar Aspect (USA) Experiment on ARGOS," AIAA Paper 2001-4664, Aug. 2001.
- ⁴⁵Ray, P. S., Wood, K. S., Wolff, M. T., Lovellette, M. N., Sheikh, S., Moon, D. S., Eikenberry, S. S., Roberts, M., Lyne, A., Jordan, C., Bloom, E. D., Tournear, D., Saz Parkinson, P., and Reilly, K., "Absolute Timing of the Crab Pulsar: X-Ray, Radio, and Optical Observations," *Bulletin of the American Astronomical Society*, Vol. 201, Dec. 2002, p. 1298.
- ⁴⁶Ray, P. S., Wood, K. S., Wolff, M. T., Lovellette, M. N., Sheikh, S., Moon, D.-S., Eikenberry, S. S., Roberts, M., Lyne, A., Jordan, C., Bloom, E. D., Tournear, D., Saz Parkinson, P., and Reilly, K., "Absolute Timing of the USA Experiment Using Pulsar Observations," American Astronomical Society, High Energy Astrophysics Div., Vol. 7, March 2003.
- ⁴⁷White, N. E., Nagase, F., and Parmar, A. N., "The Properties of X-ray Binaries," *X-Ray Binaries*, edited by W. H. G. Lewin, J. Van Paradijs, and E. P. J. Van Den Heuvel, Cambridge Univ. Press, Cambridge, England, U.K., 1995.
- ⁴⁸Taylor, J. H., "Pulsar Timing and Relativistic Gravity," *Philosophical Transactions of the Royal Society of London*, Vol. 341, Jan. 1992, pp. 117–134.
- ⁴⁹Fraser, G. W., *X-Ray Detectors In Astronomy*, Cambridge Univ. Press, Cambridge, England, U.K., 1989.
- ⁵⁰Hellings, R. W., "Relativistic Effects in Astronomical Timing Measurements," *Astronomical Journal*, Vol. 91, No. 3, 1986, pp. 650–659.
- ⁵¹Backer, D. C., and Hellings, R. W., "Pulsar Timing and General Relativity," *Annual Review of Astronomy and Astrophysics*, Vol. 24, Jan. 1986, pp. 537–575.
- ⁵²Moyer, T. D., "Transformation From Proper Time on Earth to Coordinate Time in Solar System Barycentric Space-Time Frame of Reference, Part 1," *Celestial Mechanics*, Vol. 23, Jan. 1981, pp. 33–56.
- ⁵³Moyer, T. D., "Transformation From Proper Time on Earth to Coordinate Time in Solar System Barycentric Space-Time Frame of Reference, Part 2," *Celestial Mechanics*, Vol. 23, Jan. 1981, pp. 57–68.
- ⁵⁴Thomas, J. B., "Reformulation of the Relativistic Conversion Between Coordinate Time and Atomic Time," *Astronomical Journal*, Vol. 80, No. 5, 1975, pp. 405–411.
- ⁵⁵Lorimer, D. R., "Binary and Millisecond Pulsars at the New Millennium," *Living Review in Relativity*, Max Planck Inst. for Gravitational Physics, Albert Einstein Inst., Golm, Germany, 2001.

⁵⁶Martin, C. F., Torrence, M. H., and Misner, C. W., "Relativistic Effects on an Earth-Orbiting Satellite in the Barycenter Coordinate System," *Journal of Geophysical Research*, Vol. 90, No. B11, 1985, pp. 9403–9410.

⁵⁷Richter, G. W., and Matzner, R. A., "Second-order Contributions to Relativistic Time Delay in the Parameterized Post-Newtonian Formalism," *Physical Review D: Particles and Fields*, Vol. 28, No. 12, 1983, pp. 3007–3012.

⁵⁸Seidelmann, P. K. (ed.), *Explanatory Supplement to the Astronomical Almanac*, Univ. Science Books, Sausalito, CA, 1992.

⁵⁹Manchester, R. N., and Taylor, J. H., *Pulsars*, W. H. Freeman, 1977.

⁶⁰Lyne, A. G., and Graham-Smith, F., *Pulsar Astronomy*, 2nd ed., Cambridge Univ. Press, Cambridge, England, U.K., 1998.

⁶¹Lyne, A. G., Jordan, C. A., and Roberts, M. E., "Jodrell Bank Crab Pulsar Timing Results, Monthly Ephemeris," Dept. of Physics and Astronomy, Univ. of Manchester, Manchester, England, U.K., URL: <http://www.jb.man.ac.uk/~pulsar/crab.html> [cited 13 Aug. 2002].

⁶²Ashby, N., and Allan, D. W., "Coordinate Time On and Near the Earth," *Physical Review Letters*, Vol. 53, No. 19, 1984, p. 1858.

⁶³Parkinson, B. W., and Spilker, J. J., Jr. (eds.), *Global Positioning System: Theory and Applications*, Vol. 1, AIAA, Reston, VA, 1996.

⁶⁴Parkinson, B. W., and Spilker, J. J., Jr. (eds.), *Global Positioning System: Theory and Applications*, Vol. 2, AIAA, Reston, VA, 1996.

⁶⁵Rawley, L. A., Taylor, J. H., and Davis, M. M., "Fundamental Astrome-

try and Millisecond Pulsars," *Astrophysical Journal*, Vol. 326, March 1988, pp. 947–953.

⁶⁶Kaspi, V. M., "High-Precision Timing of Millisecond Pulsars and Precision Astrometry," *Proceedings of 166th Symposium of the International Astronomical Union*, edited by E. Hog and P. Kenneth Seidelmann, International Astronomical Union, Paris, 1994, pp. 163–174.

⁶⁷Bell, J. F., "Radio Pulsar Timing," *Advances in Space Research*, Vol. 21, No. 1/2, 1998, pp. 137–147.

⁶⁸Shapiro, I. I., "Fourth Test of General Relativity," *Physical Review Letters*, Vol. 13, No. 26, 1964, pp. 789–791.

⁶⁹Battin, R. H., *An Introduction to the Mathematics and Methods of Astrodynamics*, rev. ed., AIAA, Reston, VA, 1999, Chap. 13.

⁷⁰Wood, K. S., Determan, J. R., Ray, P. S., Wolff, M. T., Budzien, S. A., Lovellette, M. N., and Titarchuk, L., "Using the Unconventional Stellar Aspect (USA) Experiment on ARGOS to Determine Atmospheric Parameters by X-Ray Occultation," *Optical Spectroscopic Techniques, Remote Sensing, and Instrumentation for Atmospheric and Space Research IV*, edited by A. M. Larar and M. G. Mlynczak, Proceedings of the SPIE—The International Society for Optical Engineering, Vol. 4485, Bellingham, WA, 2002, pp. 258–265.

⁷¹Blandford, R., and Teukolsky, S. A., "Arrival-Time Analysis for a Pulsar in a Binary System," *Astrophysical Journal*, Vol. 205, April 1976, pp. 580–591.